CHAPTER FIVE: MODELLING AND INTERPRETATION OF MAGNETIC DATA OVER THE PEEL FAULT

5.1. Introduction

Although numerous geological interpretations have been reported about the surface structure and geological history of the Peel Fault, there is limited geophysical data available to constrain the subsurface geometry on a regional scale. This thesis presents a regional scale interpretation of aeromagnetic data and five ground magnetic surveys conducted from Nundle (50 km south of Tamworth) in the south to Tarakan (90 km north of Tamworth) in the north. The strong contrast in susceptibility between the ultramafic bodies (mostly serpentinized) and surrounding rocks gives rise to prominent magnetic anomalies, which can be modelled to obtain the subsurface geometry of these bodies that are emplaced along the Peel Fault. In this chapter, on the basis of the ground magnetic data, several two dimensional magnetic models will be developed to determine the subsurface geometry of the serpentinite bodies associated with the Peel Fault. An almost three dimensional magnetic model, on the basis of the aeromagnetic data, will also be constructed to provide further insights to the subsurface structure of the Peel Fault.

5.2. Rock Properties

The magnetization of a rock, which is expressed as a vector sum is usually composed of induced and remanent components. The induced magnetization is given by multiplying the susceptibility by the magnetising field. In this study the magnetising field is the Earth's magnetic field, which is ~0.55 G in CGS, and ~55,000 nT in SI. In the modelling of a magnetic anomaly, the remanent magnetization of a body is commonly assumed to be negligible. But this is not always true, and the remanent magnetization may contribute

significantly to the total magnetization vector (Clark and Emerson, 1991; Clark, 1997). In order to determine the contribution of the remanent magnetization to the magnetic anomaly studied, and to provide better constraints for modelling, it is necessary that data both on the remanence and induced magnetization of the rocks within the study area be available.

Four to five sites were chosen to sample each serpentinite body where the magnetic survey was conducted. Cores (25 mm diameter) obtained in the field and in the laboratory were sliced into specimens with a height of 22mm to measure susceptibility and remanence. Three to five specimens were obtained from each core giving a total of about 20 specimens for each serpentinite body.

The magnetic susceptibility of the specimens was first measured in the Rock Magnetism Laboratory at the Commonwealth Scientific and Industrial Research Organisation (CSIRO) in Sydney using a transform bridge operating at 211 Hz to minimise conductivity effects (Ridley and Brown, 1980). NRM measurements of specimens were made on a horizontally mounted 2G755R DC SQUID magnetometer at CSIRO. A pilot specimen from each sample was subjected to alternating field (AF) demagnetisation in steps of 2, 3, 5, 6, 7, 8, 10, 12.5, 15, 17.5, 20, 25, 30, 40, 50, 60, 70, 80, 90 and 100 mT in this study. The AF demagnetisation results indicate that the viscous remanent magnetisation (VRM) can be removed at a field of 5 mT. After the pilot demagnetisations all specimens were demagnetised at only 5, 10, 15 mT to eliminate VRM. Following the remanent magnetization and susceptibility measurements, the Koenigsberger ratio (Q) was computed for the specimens. Figure 5.1a shows an equal angle stereonet projection of NRM of all serpentinite samples collected in this study. The results indicate that the Fisher mean NRM has a declination of 1.5°, an inclination of -69.4° and α_{95} of 18°, which is roughly consistent with present magnetic field in the study area (Dec, 11.5°; Inc -61.5°). Figure 5.1b-e show the results for each profile. It is obvious that the samples from Attunga are best grouped with α_{95} of 13.7°, then Barraba with an α_{95} of 28.8°. For the rest of

the sites, the data are not grouped enough to calculate a confident mean NRM direction, implying that remanence does not significantly contribute to the magnetisation of the serpentinite. Figure 5.2a presents an equal angle stereonet projection of the remanence direction obtained after demagnetisation at 5 mT of all serpentinite samples. The data shows a good clustering with an α_{95} of 26.8°, and a mean direction of Dec= 20.3°, Inc= -67.3°, indicating that the remanence of the samples is approximately parallel to the present magnetic field (Dec, 11.5°; Inc -61.5°). Figure 5.2 b-e shows the results for each transverse, once again, the data from Attunga shows the best grouping with an α_{95} of 16.8°, indicating that the magnetic anomaly at this site has a contribution from the remanence. The data from Barraba shows a relative clustering, also indicating a remanence contribution for the magnetic anomalies observed at that site. The data from the rest of the sites are not clustered at all, and did not provide a confident mean direction. The raw data of the rock magnetic properties of specimens collected during this study are summarised in Appendix I, including location, the intensity and directions of the natural remanent magnetization, susceptibility and Q value. A summary of the NRM direction, susceptibilities and Koenigsberger Ratios of samples collected in this study are listed table 5.1. The average susceptibilities of the serpentinite body for each transverse, range between 3021 - 5443 $\times 10^{-6}$ cgs, which is greater than both the susceptibility of serpentinite (1000-4700 $\times 10^{-6}$ cgs) in the Kootingal area (Edwards, 1996), and those (976×10^{-6} cgs) reported by Ramsay and Stanley (1976). Q values for each transverse range between 0.51 – 0.91, and are approximately consistent with those obtained in the Kootingal area (Edwards, 1996). All the mean Koenigsberger values for serpentinites for each transverse are less than 1, although individual samples did have values greater than unity. Country rocks of the Woolomin association and Tamworth Group have low susceptibilities of less than 300×10^{-6} cgs.

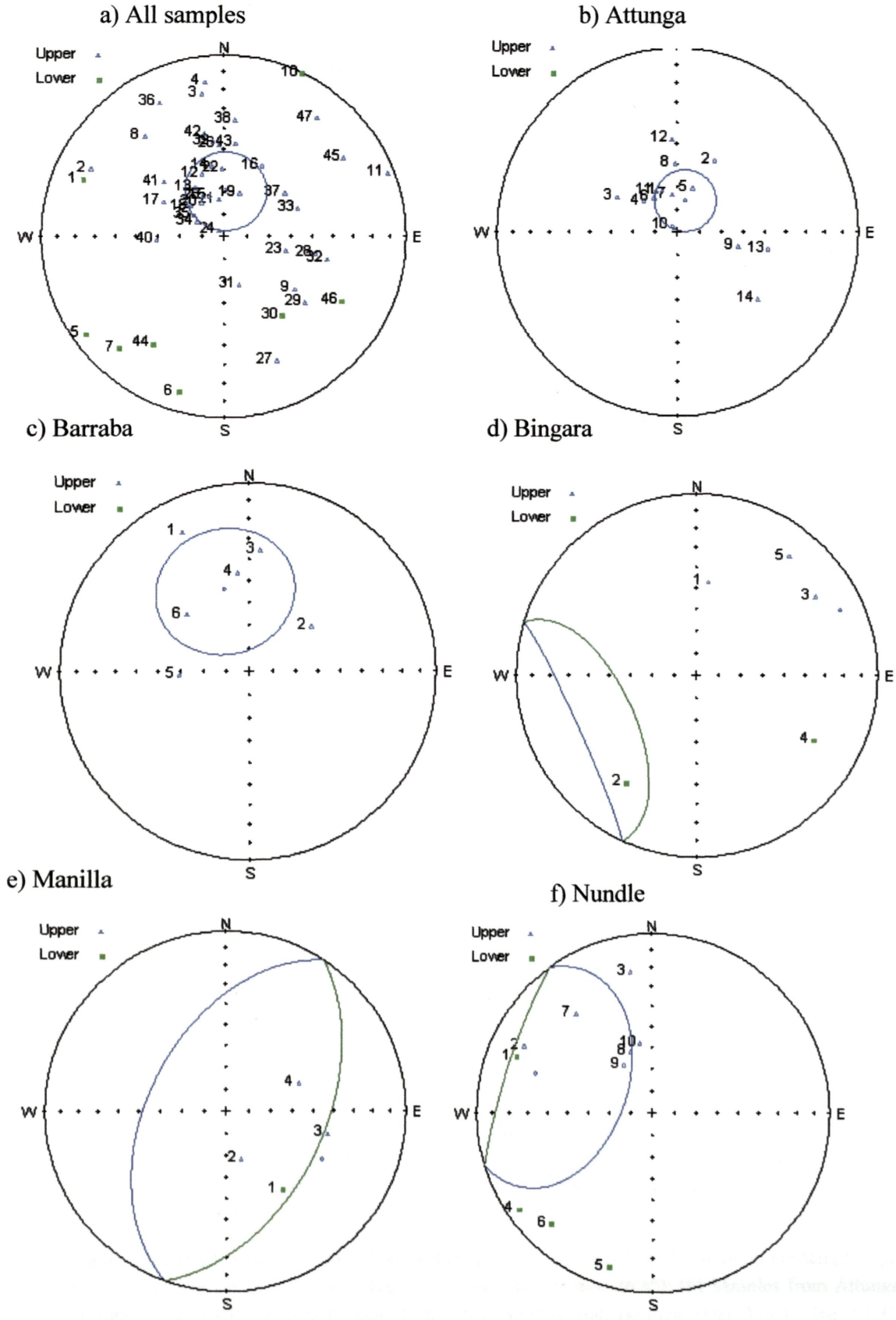

Figure 5.1 Plot of NRM directions for the serpentinite samples. (a) All Serpentinite samples (Mean = Dec, 1.5°, Inc, -69.4°, α_{95}, 18°); (b) Samples from Attunga (Mean = Dec 14.2°, Inc -75.5°, α_{95}, 13.7°); (c) Samples from Barraba, (Mean = Dec 343.3°, Inc -52.3°, α_{95}, 28.8°); (d) Samples from Bingara; (e) Samples from Manilla; (f) Samples from Nundle (Mean = Dec, 288.6°, Inc, -30.6°, α_{95}, 45.7°).

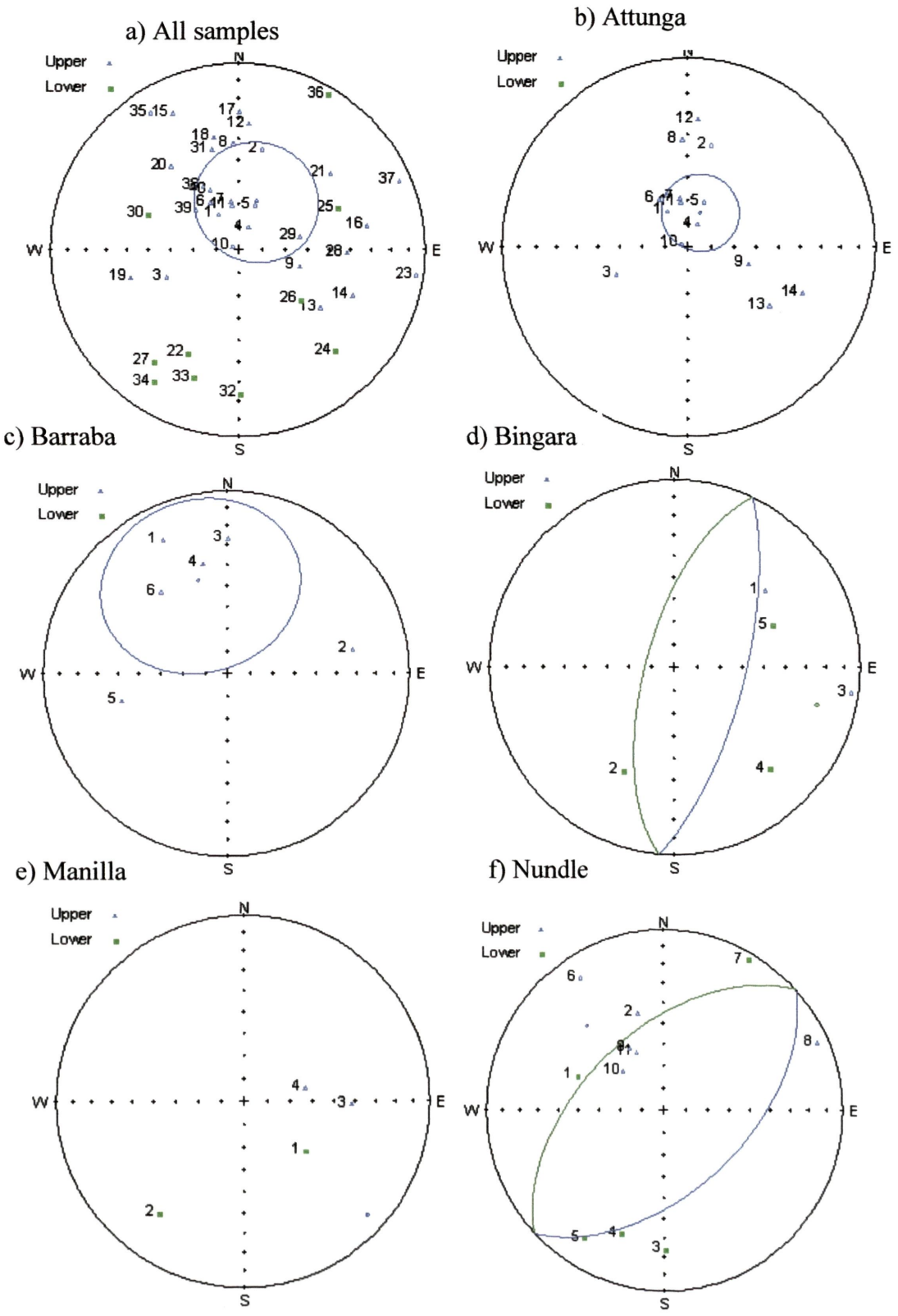

Figure 5.2 Plot of remanence directions of demagnetisation at 5 mT for the serpentinite samples. (a) All Serpentinite samples (Mean = Dec, 20.3°; Inc, -67.3°; α_{95}, 26.8°); (b) Samples from Attunga (Mean = Dec, 19.7°, Inc -74.1°, α_{95}, 16.8°); (c) Samples from Barraba, (Dec 343.3°, Inc -52.3°, α_{95}, 28.8°); (d) Samples from Bingara; (e) Samples from Manilla; (f) samples from Nundle (Dec, 317.5°, Inc, -36.7°, α_{95}, 90.3°).

Table 5.1 NRM direction, susceptibilities and Koenigsberger Ratios of samples collected in this study

Location	Name	Number	Susceptibility × 10-6 cgs	Dec (°)	Inc (°)	Intensity mA/m	Q value	Easting (AMG56)	North (AMG56)
Nundle									
	SP01	2	3060.527	292.3	17.7	1274.4	0.833	327790	6515576
	SP02	2	4116.929	297.3	-19.3	562.615	0.273	327790	6515576
	SP03	9	4145.535	351.1	-21.5	4384.322	2.115	327781	6515596
***	SP04	9	3728.742	352.9	-15.3	24220.67	12.991	327781	6515596
	SP05	1	3997.778	234.94	7.51	1971.5	0.986	327776	6515666
	SP06	1	3324.632	196.57	11.81	2204.6	1.326	327776	6515666
	SP07	2	3737.663	223.2	16.7	2584.375	1.383	327776	6515666
	SP08	1	5342.94	321.9	-30.45	1826	0.684	327732	6515826
***	SP09	1	5775.653	126.93	-50.35	10175	3.523	327732	6515826
***	SP10	1	12480.67	25.35	0.63	21267	3.408	327686	6515839
***	SP11	1	3261.208	68.65	-3.97	6374.5	3.909	327686	6515839
	SP13	1	5630.59	340.42	-60.01	1920.8	0.682	327654	6515895
	SP14	1	6209.549	329.2	-64.28	1019.6	0.635	327654	6515895
	SP15	1	4598.734	349.91	-57.49	1554.3	0.676	327654	6515895
Average			4416.487				0.959		
Std			1022.561				0.524		
Attunga									
	SP16	1	6707.574	339.66	-70.4	3133.7	0.934	300232	6585583
	SP17	3	7022.236	27.8	-53.6	2121.867	0.604	300232	6585583
	SP18	2	6674.327	299.8	-58.6	2579.35	0.773	300232	6585583
	SP19	1	7919.79	312.18	-69.77	1412.1	0.357	300232	6585583
	SP20	1	5539.86	18.92	-69.36	1531	0.553	300232	6585583
	SP21	1	6647.53	325.93	-71.56	1829.9	0.550	300232	6585583
	SP22	1	5136.813	351.36	-73.17	3442.3	1.340	300232	6585583
	SP23	2	5428.801	358.1	-59.3	2841.55	1.047	300098	6585501
	SP24	1	3265.792	103.03	-61.9	2443.6	1.496	300098	6585501
	SP25	1	5529.119	319.77	-86.3	4792.3	1.733	300098	6585501
	SP26	1	5034.517	331.73	-69.51	2071.8	0.823	300098	6585501
	SP27	6	4432.929	356.5	-48	1578.283	0.712	300787	6586753
***	SP28	3	15.365	157.4	-26.8	0.130825	0.017	300787	6586753
	SP29	13	4184.243	100.2	-47.9	1688.065	0.807	300851	6586678
	SP30	8	2682.745	129.3	-42.3	1307.829	0.975	300851	6586678
Average			5443.305				0.908		
Std			1478.987				0.389		
Manilla									
	SP31	12	3154.009	144.5	45.8	1556.977	0.987	296565	6608712
	SP32	6	2356.406	163.6	-67.3	257.6647	0.219	296565	6608712
	SP33	7	3285.143	102.5	-42	615.6471	0.375	296565	6608712

	SP34	11	3291.481	68.6	-54.6	761.5527	0.463	296565	6608712
***	SP35	6	488.3252	298.9	-76.1	217.837	0.892	296661	6606614
***	SP36	6	680.9597	304.5	-73.5	443.3683	1.302	296661	6606614
Average			3021.76				0.511		
Std			448.072				0.333		
Barraba									
	SP37	6	1719.055	334.4	-19.2	951.0367	1.106	281148	6634453
	SP40	3	2508.491	54	-56.5	1024.117	0.817	281148	6634453
	SP41	15	1746.769	365.2	-35.6	781.428	0.895	281281	6634475
	SP42	12	3193.596	353.3	-46	2552.069	1.598	281281	6634475
	SP43	7	4720.33	267	-59.6	1593.041	0.675	281281	6634475
	SP44	12	4838.755	312.4	-53.1	1672.045	0.691	283093	6634579
***	SP45	14	312.0344	349.1	-41.6	220.3633	1.412	283093	6634579
Average			3121.166				0.964		
Std			1395.918				0.348		
Bingara									
	SP46	3	4302.888	6.9	-47.1	1196.7	0.556	272721	6665432
	SP48	6	3272.122	213.6	30	1744.3	1.066	272721	6665432
	SP49	13	5292.23	56.6	-22.6	2306.303	0.872	270134	6663669
	SP50	10	3235.545	118.9	27.3	578.413	0.358	270134	6663669
	SP51	7	3414.939	37.8	-18.2	951.3214	0.557	270134	6663669
Average			3903.545				0.682		
Std			890.445				0.283		

Note: The samples with *** were excluded from calculation of the average susceptibility and/or Q value due to the weathering of the sample or the effect of lightning on the sample. Explanation of Table 5.1 headings: Location, for sampled location, Number, for number of measured specimen, Dec and Inc, for measured direction of natural remanent magnetization, Q, for Koenigsberger ratio.

Table 5.2 Local geomagnetic parameters

Parameters Transverses	Magnetic field intensity (nT)	Magnetic Field Dec (°)	Magnetic Field Inc (°)	Line Length	Line Average Direction (True)
Tarakan	55402	11.2	-60.8	9.1 km	51°
Barraba	55545	11.3	-61.1	12.4 km	43°
Manilla	55651	11.4	-61.3	2.9 km	102°
Attunga	55777	11.5	-61.5	11.1 km	31°
Nundle	56037	11.8	-62.1	9.5 km	86°

5.3. Modelling results of ground magnetic data over the Peel anomaly

The magnetic data collected across the Peel Fault was modelled using Modelvision Pro 5.0 ^{TM} – an interactive gravity and magnetic modelling package produced by Encom Technology. The program calculates and compares the theoretical magnetic responses of a structural model with profiles of the observed data. The degree of misfit is quantified by calculated root-mean-square (rms) error, and the user can interactively modify the model to get the best fit. A root-mean square error of five was the target for the degree of misfit for the accepted models of each transverse and was achieved in all cases. Local geomagnetic parameters for each traverse are shown in Table 5.2.

An upward continuation filter of 30 m was applied to all ground magnetic data before the data was modelled. The upward continuation filter transforms the potential field data measured on one surface to a higher surface, and by doing so, reduces anomalies due to artificial materials and minor topographic effects on the magnetic anomaly, which also functions as a high frequency filter. The anomalies were initially modelled by forward calculation using a magnetized tabular body, and then inversion was done to produce a best-fit model for the observed anomalies.

Line Tarakan, Bingara

The line Tarankan is in the northern part of the study area (Figure 4.8) and was surveyed along an east-north-east trending track normal to the strike of the outcropped serpentinite. The observed data are shown in Figure 5.3. The major peak associated with the serpentinite outcrop occurs between 4200-5600 m along the profile. The country rocks of the serpentinite body are the non-magnetic Early Permian Tarakan Formation composed of quartzose and lithic sandstone with minor mudstone and siltstone to the west and the non-magnetic Middle? Silurian-Late Devonian Nangahrah Formation composed chiefly of cherts, siliceous mudrocks

to the east (Brown et al, 1992). As a concrete bridge at 4000m generated the magnetic anomaly at that location, no attempt was made to model the data from this part of the section. To the east, no visible magnetic sources correspond to the group of higher readings at 6400 m on the horizontal axis; a higher susceptibility body (serpentinite) below surface is assumed to be responsible for this anomaly.

The magnetic data from this traverse were modelled with an assumption of magnetic induction only because the remanence data of samples from this site are not grouped enough to produce a consistent mean NRM direction and the Q value for the Tarakan samples is only 0.68. The average measured bulk susceptibility of 3903 $\times$ 10^{-6} cgs of Tarakan serpentinite samples was initially used to model the Peel anomaly over this transverse. The inversed best-fit model indicates a surface width approximately equal to the observed outcrop width (Figure 5.3a) and dipping steeply to the east. In order to match the observed data, the depth to the base of the serpentinite body needed to be at least 1300 m. However, no constraint could be put on the maximum depth to the base of the serpentinite, as the degree of fit does not change significantly if the bodies are modelled extending to a much greater depth. If the susceptibility is taken as 4900$\times$ 10^{-6} then a depth to the base of the serpentinite of less than 1 km will produce a good fit to the data (Figure 5.3b).

A west dipping body was also modelled to see if it was possible for a west dipping serpentinite body could produce the anomaly. Figure 5.3c shows the calculated anomaly due to a body that dips to the west, and the shape of the calculated anomaly is more symmetrical than that of the real anomaly and it is concluded that a body dipping to west does not produce an anomaly to match the observed magnetic data.

In addition, a small body with susceptibility of 6994 $\times$ 10^{-6} cgs, about the highest value measured, was introduced to match the highest peak of the observed data, reflecting the heterogeneity of the susceptibility within the modelled serpentinite body (Figure 5.3a). For

the anomaly at 6400 m, an east dipping body with an average susceptibility of 3903× 10^{-6} cgs was used to match observed data. No surface geological evidence for this constructed tabular body is known to outcrop, probably indicating a sliver of serpentinite.

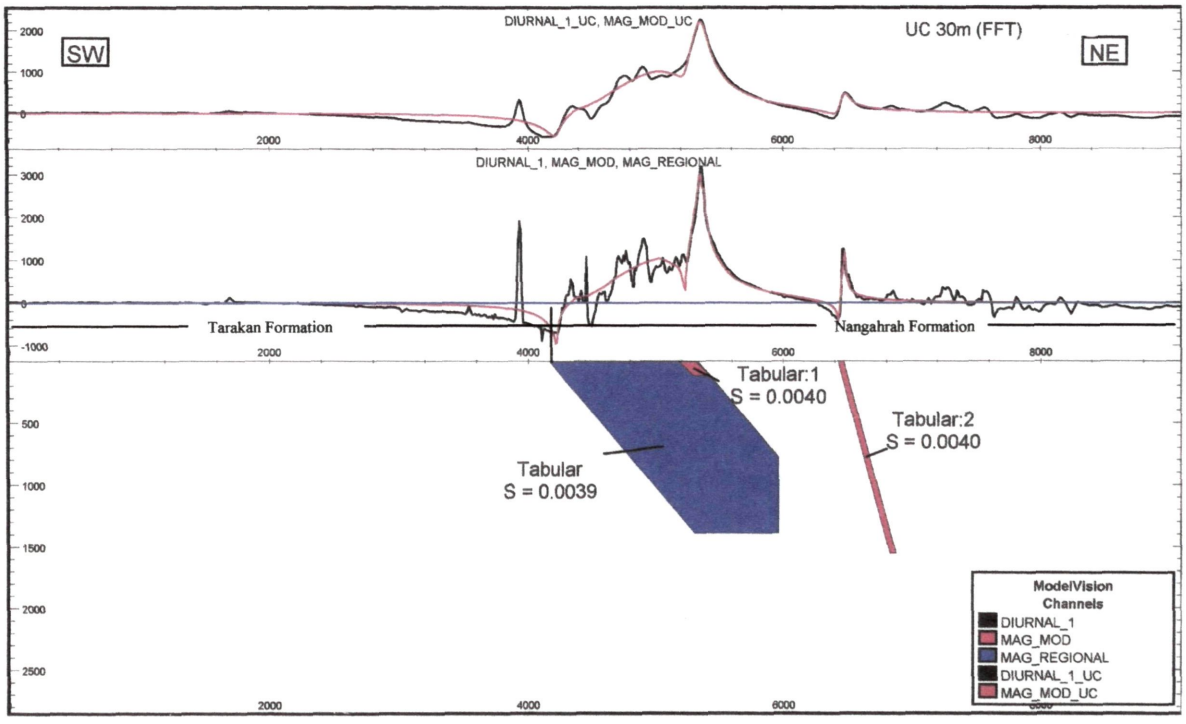

Figure 5.3a. 2-D magnetic model along the Tarakan traverse, Bingara (cross-section view). The main tabular body dips to the east at 53° with an azimuth of 348° and a depth extent of 1.4 km, V/H=1. The red line represents the modelled magnetic response and the black line the observed data. The average measured value of susceptibility was used for modelling. See Figure 4.8 for location of cross-section.

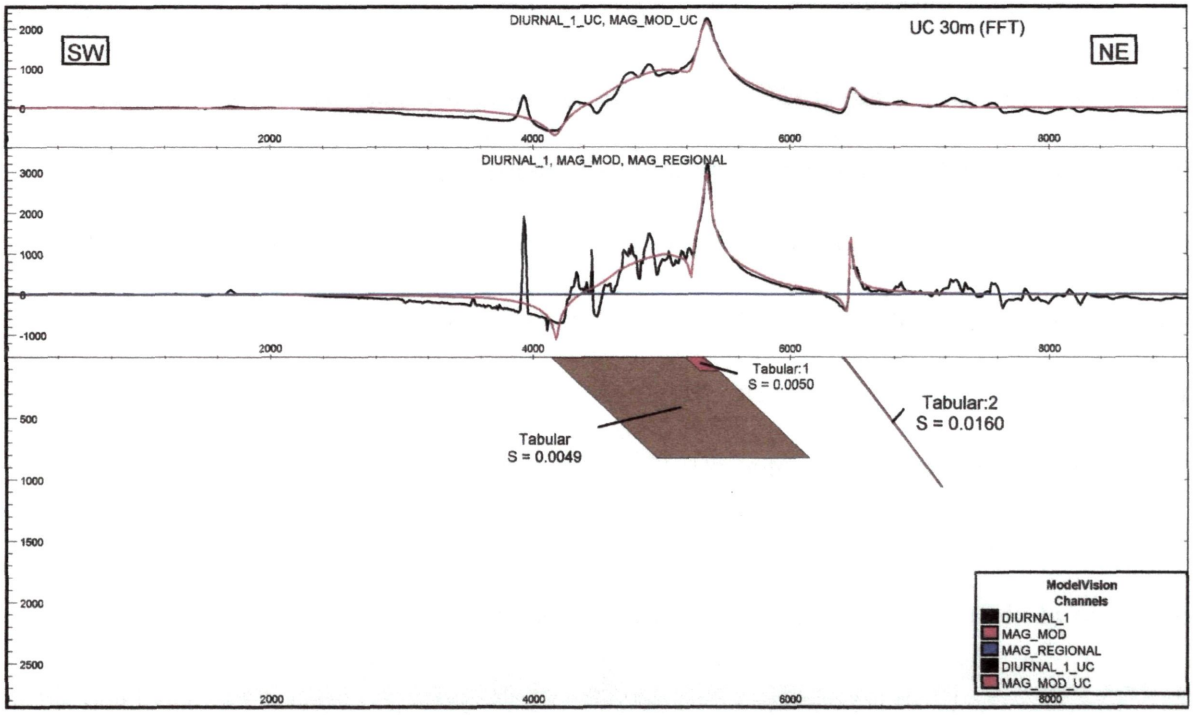

Figure 5.3b. 2-D magnetic model along the Tarakan traverse, Bingara (cross-section view). The main tabular body dips to the east at 46° with an azimuth of 338° and a depth extent of 800m, V/H=1. A higher susceptibility was used. See Figure 4.8 for location of cross-section.

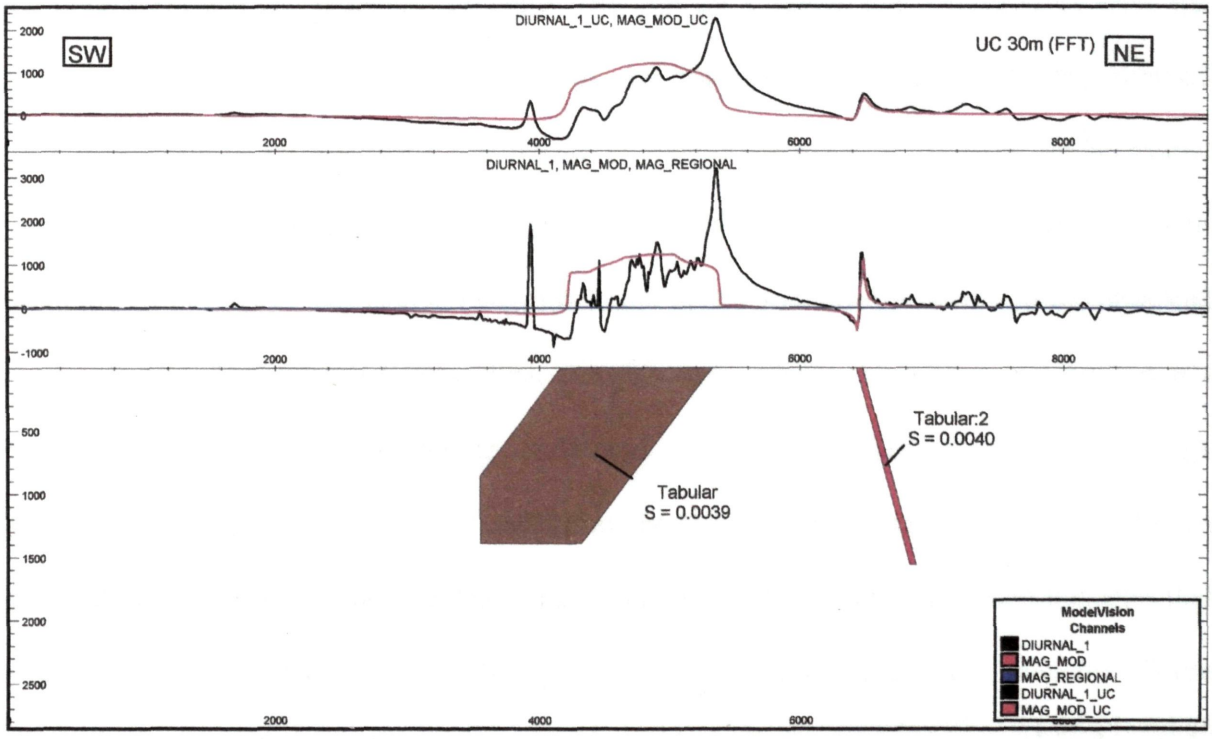

Figure 5.3c. 2-D magnetic model along the Tarakan traverse, Bingara (cross-section view), showing the good fit for a west dipping body. The main tabular body dips to west at 57° with an azimuth of 348° and a depth extent of 1.4 km, V/H=1. See Figure 4.8 for location of cross-section.

Line Manilla

The Manilla line is located east of the town of Manilla (Figure 4.8), and was surveyed along an east-west dirt road, that crosses the geological boundary between the Tablelands Complex and the Tamworth Belt (Brown et al, 1992). The non-magnetic Early Carboniferous Namoi Formation composed of mudstone and siltstone outcrops to the west of the Peel Fault and the Middle? Silurian-Late Devonian Nangahrah Formation composed chiefly of cherts, siliceous mudrocks to the east (Brown et al, 1992). No outcropping serpentinite occurs along this traverse perhaps due to the alluvium cover. Serpentinites, however, outcrop along a splay of the Peel Fault 2 km east of the geological boundary, and make it possible to obtain rock properties of serpentinites for magnetic modelling. The anomaly between 1500 and 2000 m is assumed to result from subsurface serpentinite bodies (Figure 5.4). Modelling of the observed data started with matching the main features of the upward continued data and then modelling the near surface high frequency anomaly. The average value of the susceptibility from the nearest serpentinite outcrop is 3022×10^{-6} cgs, and this value was used to model the observed data. Modelling using this value was unable to explain the peak. In addition, the measured remanence of the samples from the nearest serpentinite outcrop does not show a tight grouping of the NRM direction (Figure 5.4e), and hence does not contribute to the observed magnetic data. This case indicates either that this susceptibility of 3022×10^{-6} cgs can not represent the modelled serpentinite body and surveyed serpentinite body has a high susceptibility or that the samples collected from the nearest serpentinite outcrop are weathered and at depth the serpentinite body has a higher susceptibility. An inverted result indicates that a susceptibility of 6926×10^{-6} cgs brings a match to the amplitude of the anomaly (Figure 5.4a). The susceptibility still falls into the range of the susceptibility measured in this study (Table 5.1). The inverted body dips to east at an angle of 86° with an azimuth of 13°. A minimum depth of 2.5 km to the base of serpentinite body is required to fit the observed

magnetic anomaly. Depths of 2.5 km or deeper to the base of the modelled body produces very similar magnetic responses. It is therefore difficult to define the exact depth extension of the serpentinite body.

The bodies dipping to the west were modelled to evaluate the difference between the best fit model and the possibility of the subsurface geometry of the serpentinite body as proposed by the interpretation of seismic data (Korsch et al., 1993a, 1997). Figure 5.4b shows that a west dipping body dipping at an angle of 64° produced a similar magnetic response as that of the best-fit model. This body has an azimuth of 343°, a depth extension of 4 km and a susceptibility of 6000×10^{-6} cgs.

Only, if the susceptibility of a constructed body was increased to 17000×10^{-6} cgs, could the depth to the base of serpentinite body be less than 1 km. This value is too high when compared to the measured values and there is no available evidence supporting this assumption. Using the measured range of susceptibility values of the serpentinite samples from the nearest serpentinite outcrop, a body with a depth of less than1 km cannot produce the anomaly.

In the following modelling stage, a near surface body was introduced to match the high frequency features of the magnetic data. A peak west of the highest peak of the magnetic data was modelled as a west-dipping dyke-like body. A blind body with susceptibility of 5700×10^{-6} cgs extends westward for about 80m and may be a gabbro or dolerite sill as observed 25 km south at Attunga (Cawood, 1980). No outcrops of such bodies were reported due to alluvium cover. The modelled depth extent of the main serpentinite body could be reduced to less than 1 km with a susceptibility of 3900×10^{-6} cgs, which falls in the range of the measured susceptibility of specimens collected from serpentinite outcrop 2 km east of the surveyed traverse (Figure 5.4c). It would seem that the serpentinite body may extend only the

depth of about 1 km in this traverse with a contribution of high magnetic sill, the data does not allow a measurement of the depth to the base of the serpentinite.

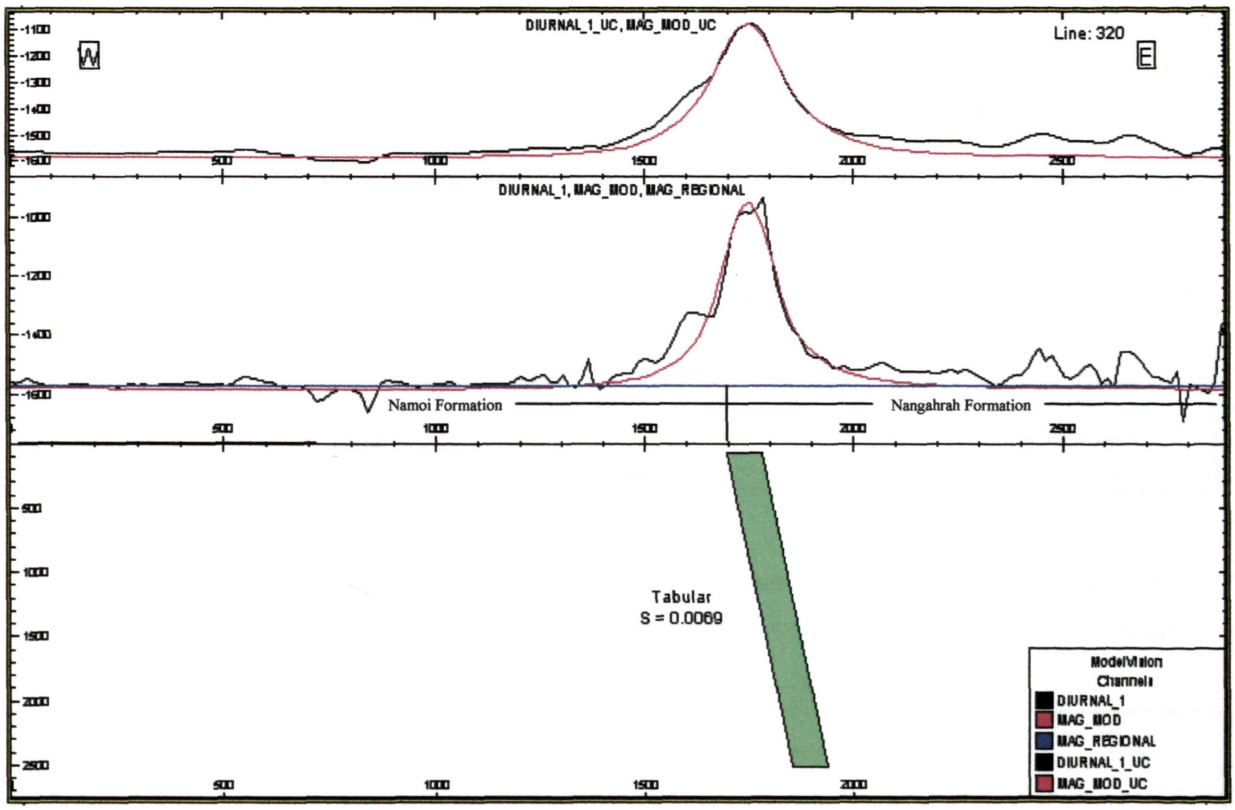

Figure 5.4a. 2-D magnetic model along the Manilla traverse (cross-section view). The tabular body dips to the east at 86° with an azimuth of 13° and a depth extent of 2.5 km, V/H =0.25. See Figure 4.8 for location of cross-section.

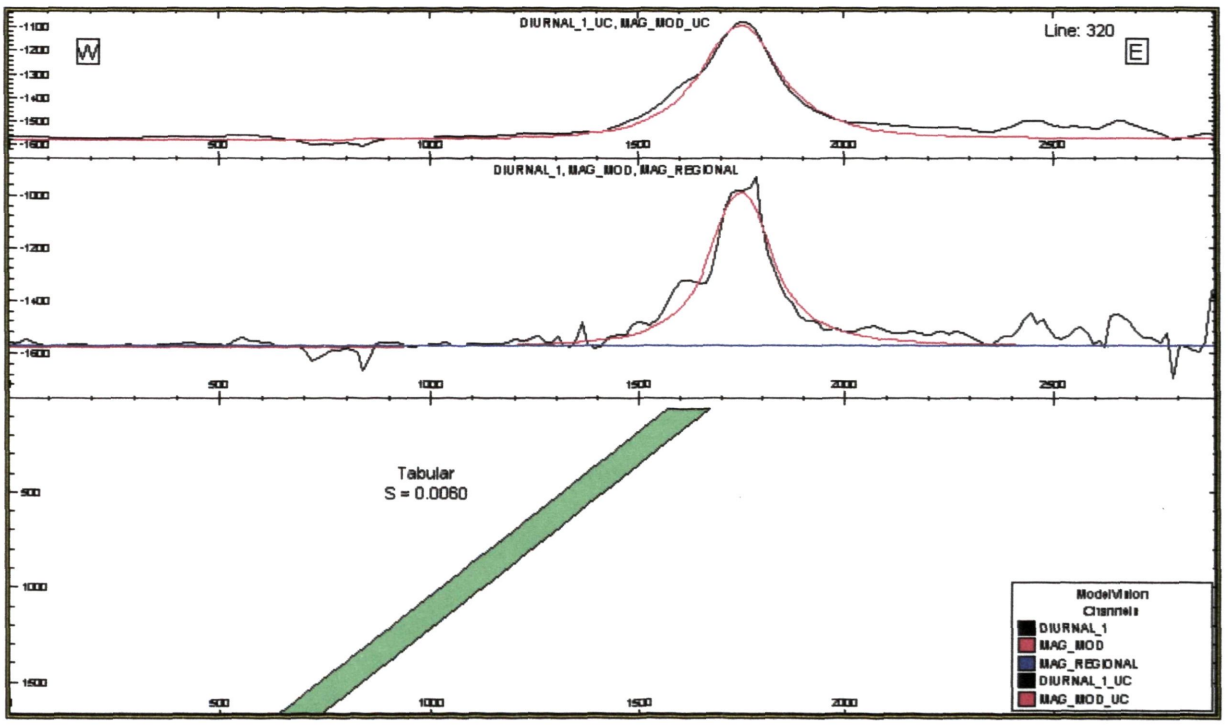

Figure 5.4b. 2-D magnetic model along the Manilla traverse (cross-section view). The main tabular body dips to the west at 64° with an azimuth of 343° and a depth extent of 3 km, V/H =0.5. See Figure 4.8 for location of cross-section.

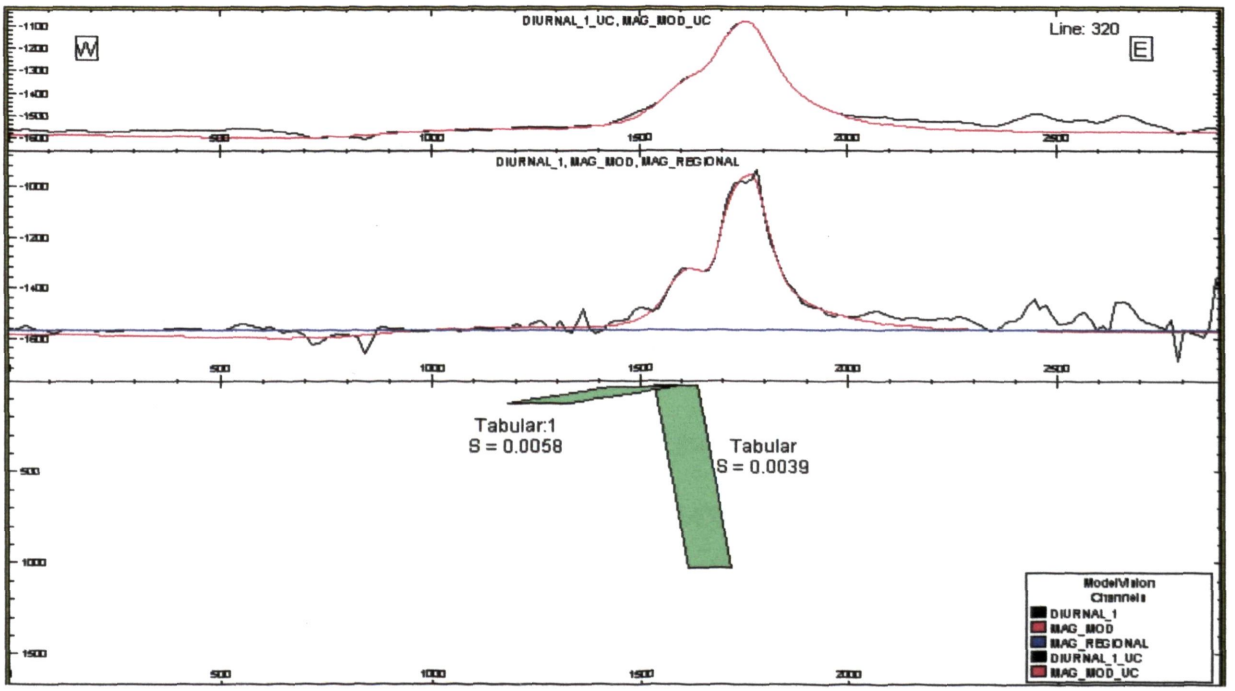

Figure 5.4c. 2-D magnetic model along the Manilla traverse (cross-section view). The main tabular body dips to the east at 86° with an azimuth of 348° and a depth extent of 1 km. The small body which dips west shallowly, probably represents a stretched serpentinite body, V/H =0.5. See Figure 4.8 for location of cross-section.

Line Glendhu, Attunga

This magnetic transverse was conducted through the Glendhu Property, east of Attunga (Figure 4.8 and Figure 5.5a). The data are presented in Figure 5.5 with the major anomaly (3200 – 4000 m) produced by serpentinite bodies, which outcrop between 3400-4200 m along the surveyed road. The country rocks to the west of the serpentinite are the non-magnetic Early Permian Kensington Formation composed of lithic wacke, siltstone and black shale, and the Early Late Devonian Tamworth Group. The Early? Carboniferous non-magnetic Wisemans Arm Formation composed of lithic wacke, siltstone and conglomerate with minor chert and limestone lies immediately east of the main serpentinite body (Shaw and Flood, 1974; Leitch, 1979; Leitch and Cawood, 1980; Brown et al, 1992). To the east of the main anomaly, the peaks at 5500m corresponds to a small serpentinite outcrop within the Wisemans Arm Formation, the anomalies at 4400m, 4800m may be also produced by near surface serpentinite bodies, but no outcrops are known. A fence produces the group of anomalies near the eastern end of the transverse and no attempt is made to model the data from that part of the transverse.

Modelling of the observed data started with matching the main features of the upward continued data and then modelling the near surface high frequency anomaly. The constructed serpentinite body was assumed to have a homogeneous susceptibility and represent the overall magnetic feature of the serpentinite body. Once a good match between the calculated profile and the upward continued data was obtained, several near surface small bodies were introduced to match the observed high frequency features of the main anomaly, and the anomalies (4400m, 4800m, 5500m) east of the main amplitude. The near surface bodies approximately correspond to the serpentinite outcrops of the road cut. It is emphasised is that the near surface body is assumed to have a homogenous susceptibility. The gaps between the near surface serpentinite bodies may reflect the susceptibility heterogeneity within the

modelled serpentinite body, where less magnetic material occurs with more magnetic material. The average value of the measured susceptibility of the serpentinite outcrop at Glendhu, Attunga of 5443 × 10^{-6} cgs is not sufficiently high to produce the major anomaly over this transverse. However, the study of the rock properties of the samples from this site shows that the remanence direction after AF demagnetisation at 5 mT grouped at a declination of 19.7° and inclination of -74.1° with an α_{95} of 16.8° (Figure 5.2b), approximately consistent with present magnetic field in Attunga (Dec, 11.5°; Inc, -62°). The samples from Attunga have a mean Koenigsberger ratio of 0.9 (Table 5.1), thus the remanance does contribute to the observed anomalies. Modelling of the observed data started with a single tabular body. After a preliminary fit was achieved between the upward continued data and the calculated curve by trial and error, inversion of the magnetic data was conducted to get a best match. Modelling results (Figure 5.5b) indicates that a susceptibility of 10000 × 10^{-6} cgs is required for the single tabular body to fit the major peak. A susceptibility of 10000 × 10^{-6} cgs is approximately equal the calculated susceptibility of 10777× 10^{-6} cgs incorporating the contribution of both the induction and remanance with a Q value of 0.97. The model of the best fit shows the tabular body has a minimum depth extent of 2.5 km, and a dip to the east of 85° (Figure 5.5b). The modelling result showed that the depth extent to the base of serpentinite body of 2.5 km is a minimum as extending the body further than 2.5 km did not reduce the degree of fit to the observed data and no constraint can be placed on the maximum depth to the base of the serpentinite.

A body with depth of less than 1 km would only produce a good fit for the major anomaly if an extremely high susceptibility of 18000 × 10^{-6} cgs was assumed (Figure 5.5c). No available evidence supports this unreasonable assumption. Alternatively, Figure 5.5d illustrates the anomaly produced by a body dipping steeply to the west, showing that a body with steep westward dip can make a good fit for the observed magnetic anomaly.

At last stage of modelling of the observed data, to obtain a better fit to the high frequency features, small near-surface bodies are introduced (Figure 5.5e). In this case dip of the best-fit tabular bodies is steeply dipping to the east.

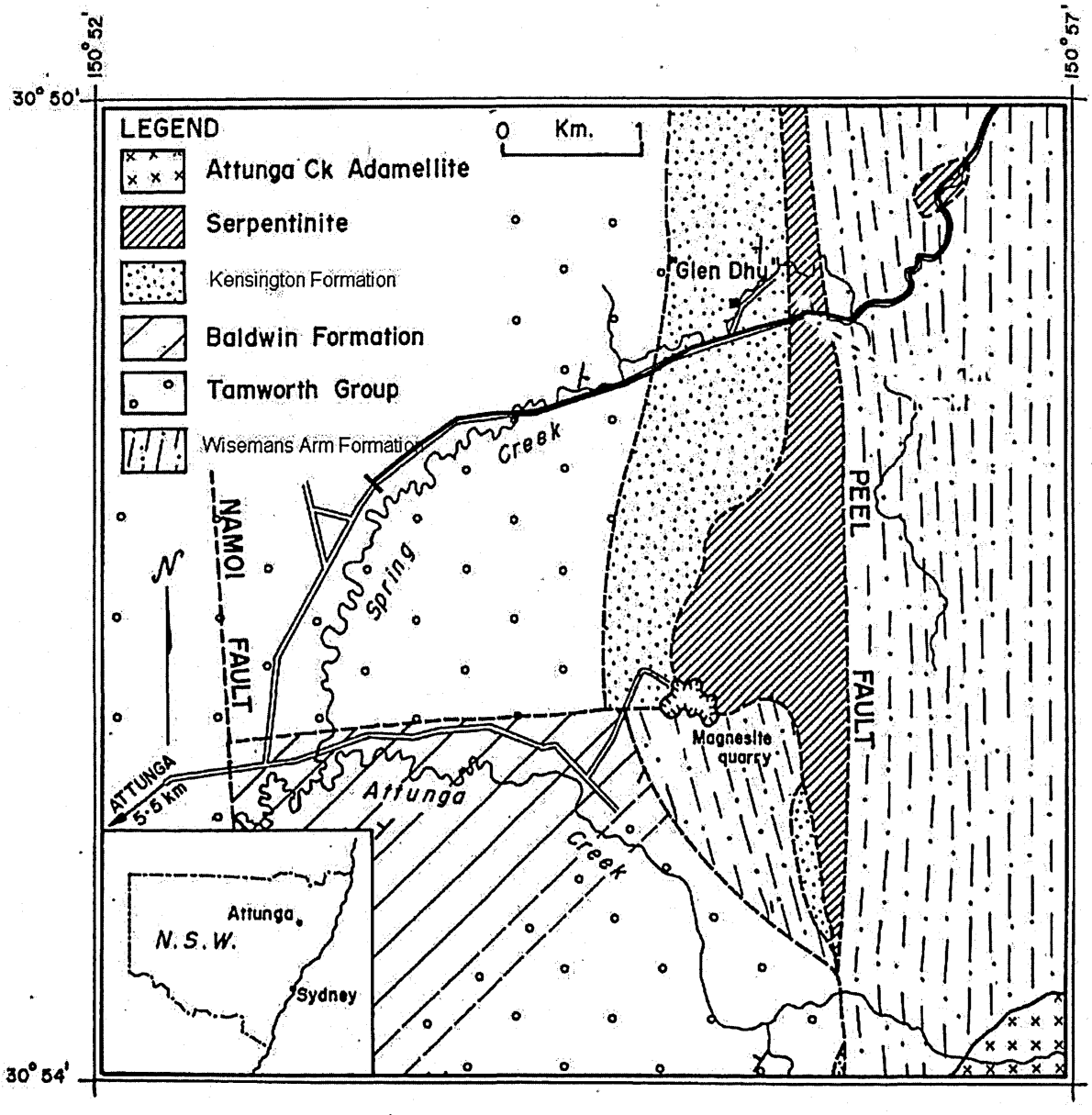

Figure 5.5a Location of Glen Dhu magnetic traverse (thick black line). Also shown is the geology along the traverse (Modified from Shaw and Flood, 1974; Leitch and Cawood, 1980)

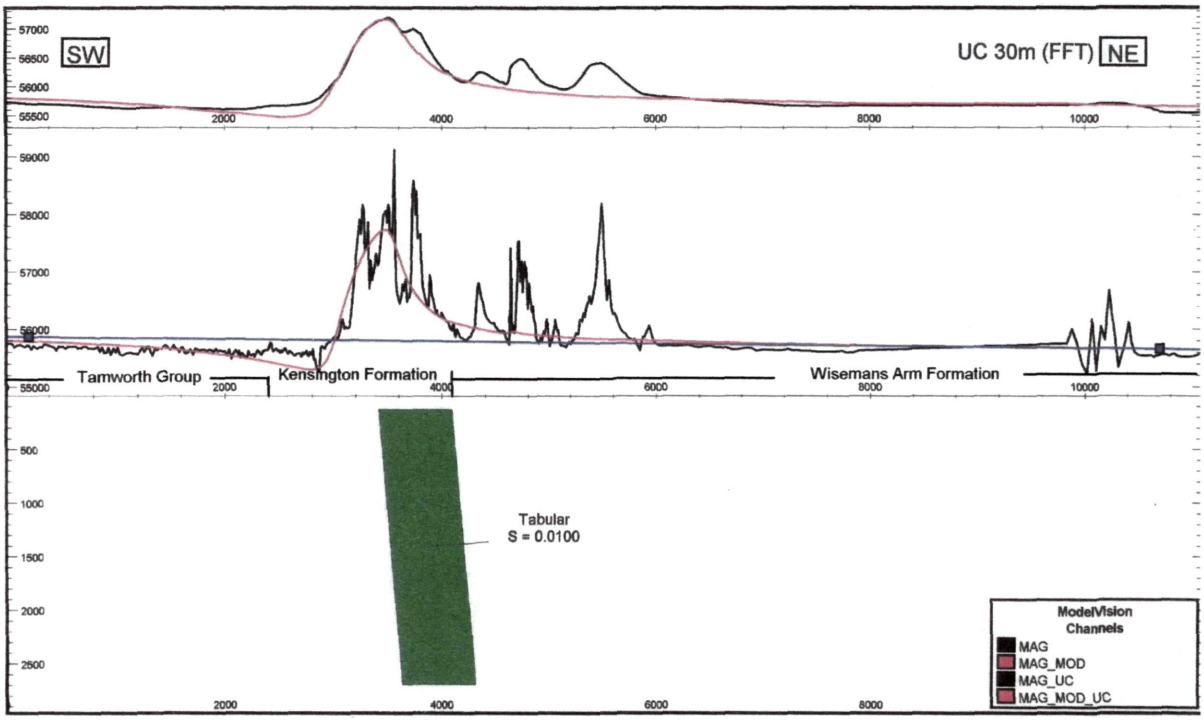

Figure 5.5b. 2-D magnetic model along the Glendhu traverse (cross-section view). A tabular body was used to match the observed data, which dips to the east at 86° with an azimuth of 345° and a depth extent of 2.5 km, V/H =1. See Figure 4.8 for location of cross-section.

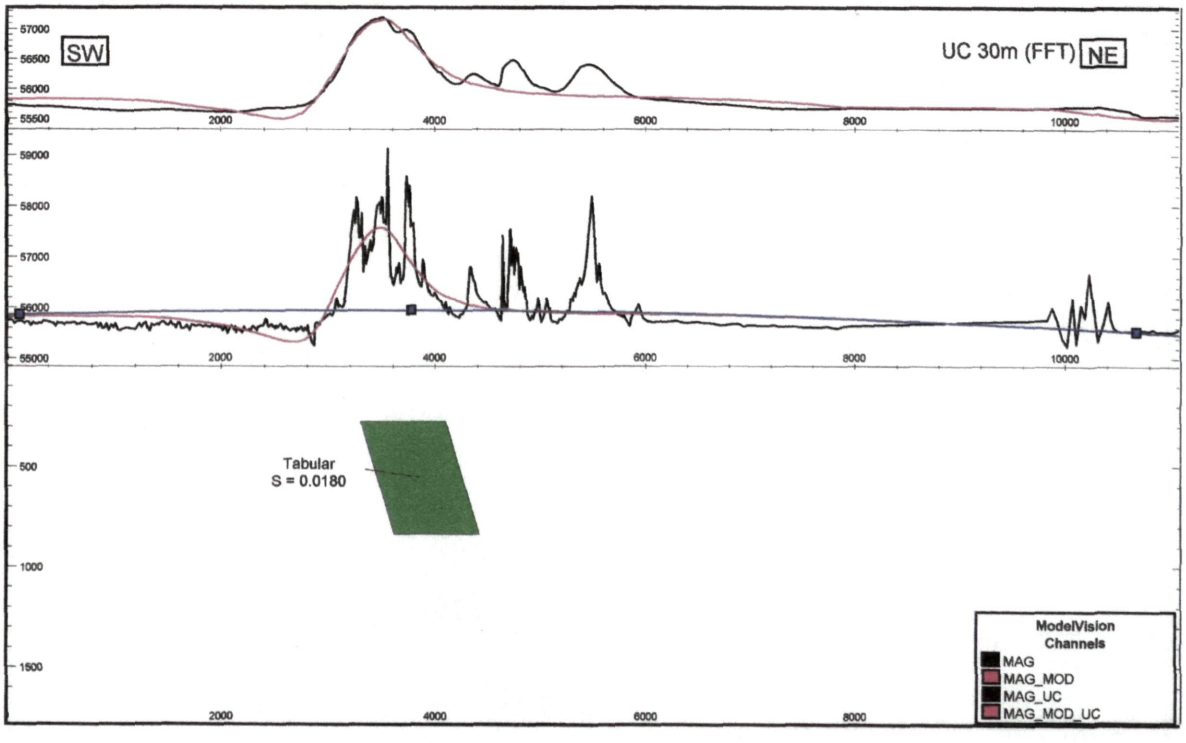

Figure 5.5c. 2-D magnetic model along the Glendhu traverse (cross-section view). A tabular body with a depth extent of less than 1 km was used to match the observed data, which dips to the east at 65° with an azimuth of 335°, and has a high susceptibility, V/H =2. See Figure 4.8 for location of cross-section.

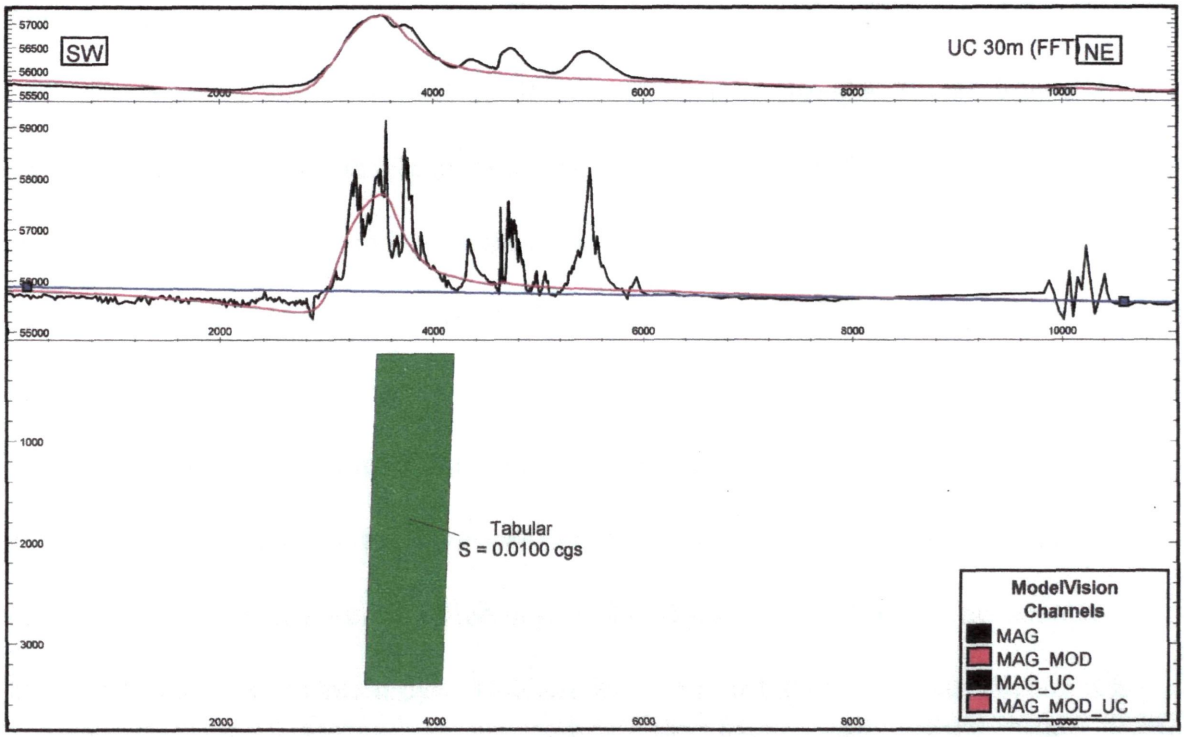

Figure 5.5d. 2-D magnetic model along the Glendhu traverse (cross-section view). The tabular body steeply dips to the west at 88° with a depth extent of 3.2 km and an azimuth of 335°, V/H =2. See Figure 4.8 for location of cross-section.

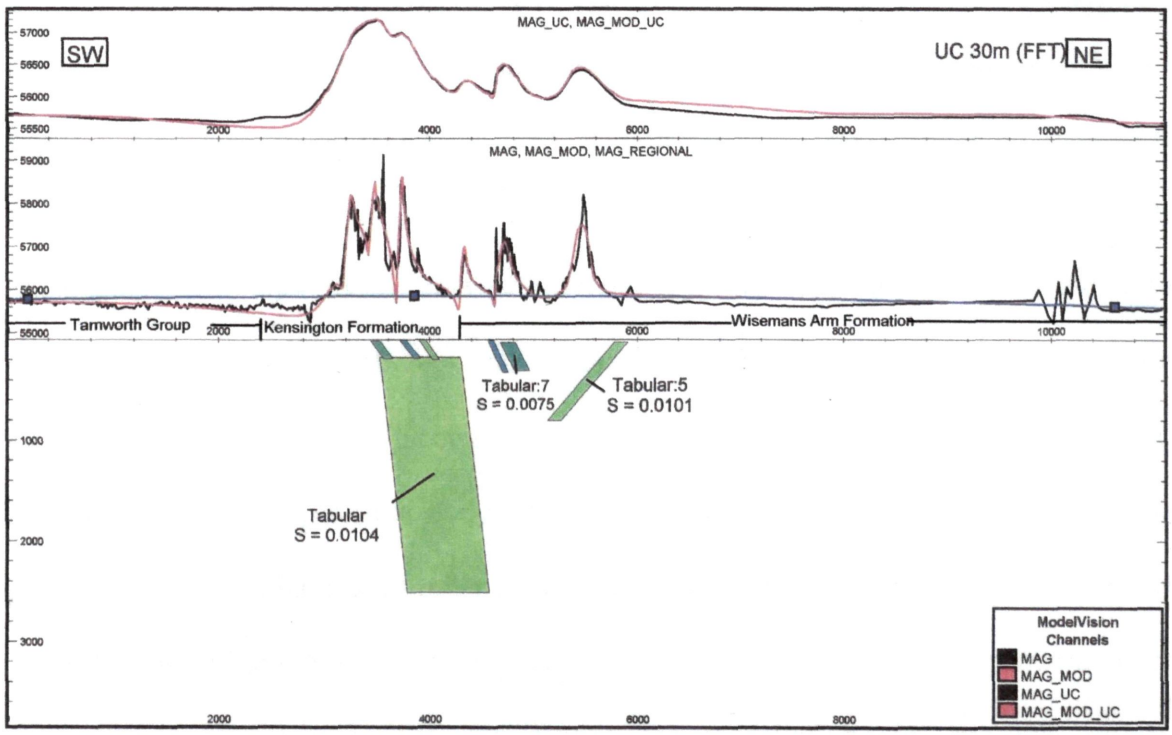

Figure 5.5e. 2-D magnetic model along the Glendhu traverse (cross-section view). Small near-surface bodies are introduced to match the high-frequency detail caused by near-surface features. The shape and dip of the main tabular bodies remain unchanged as seen in Figure 5.5a, V/H =1. See Figure 4.8 for location of cross-section.

Line Barraba

The Barraba line is located at Woodsreef, east of Barraba Town (Figure 4.8). The magnetic data is shown in Figure 5.6. The main anomaly in Figure 5.6 has amplitude of approximately 3800 nT, and correlates well with the location of the serpentinite outcrop mapped by Blake and Murchey (1988a, b). Located to the west of the serpentinite is the non-magnetic Early Carboniferous Namoi Formation composed of mudstone and siltstone with minor limestone. The Middle? Silurian-Late Devonian non-magnetic Nangahrah Formation composed of cherts, siliceous mudrocks and minor limestone forms the eastern country rock of the serpentinite (Blake and Murchey, 1988; Brown et al, 1992). The anomaly is best modelled as a complex multi dyke structure as shown in Figure 5.6a, but whether it is dykes or serpentinite with inclusions of other rocks is not clear. The average measured surface serpentinite susceptibility of 3200×10^{-6} cgs is too low to fit the observed magnetic anomaly using a body with the same width as the surface outcrop. The remanance measurements of the samples from Barraba show that the remanence directions of the samples at 5 mT approximately parallel the present magnetic field in Barraba. The Q value of the samples from Barraba ranges from 0.67 to 1.59 with a mean value of 0.97, indicating a significant remanance contribution to the observed magnetic anomaly. The inverted results indicate that a susceptibility of 8000×10^{-6} cgs was needed for the two major bodies, which is a little bit higher than the susceptibility incorporating magnetic induction and remanance of the samples, implying that the serpentinite body has a slightly high susceptibility at depth. A small polygon component having a similar susceptibility of 8400×10^{-6} cgs is used to obtain a good fit in the east (Figure 5.6a). The modelled bodies all correspond to the serpentinite outcrops along the surveyed line. The gap among the modelled bodies probably reflects a heterogeneous susceptibility within the real serpentinite bodies, which could be partially

serpentinised peridotite or blocks of other rocks. The best fit for the observed data requires a minimum depth extension of 2.5 km to the base of the two major serpentinite bodies.

When the depth extension to the base of serpentinite is reduced to less than 1 km, susceptibility four times that measured is needed to fit the observed anomaly (Figure 5.6b). No available evidence indicates that this value is realistic. In addition, the gaps between the surface and the top of the two modelled serpentinite bodies are not consistent with the fact that the serpentinite bodies outcropped along the surveyed line, indicating this model is not geologically realistic. Alternatively a simple single body model also produces a reasonable fit for the anomaly (Figure 5.6c) without effort to match the observed high frequency features. The best fit using a single body indicates that the body dips steeply to the east and has a susceptibility of 8200 × 10^{-6} cgs.

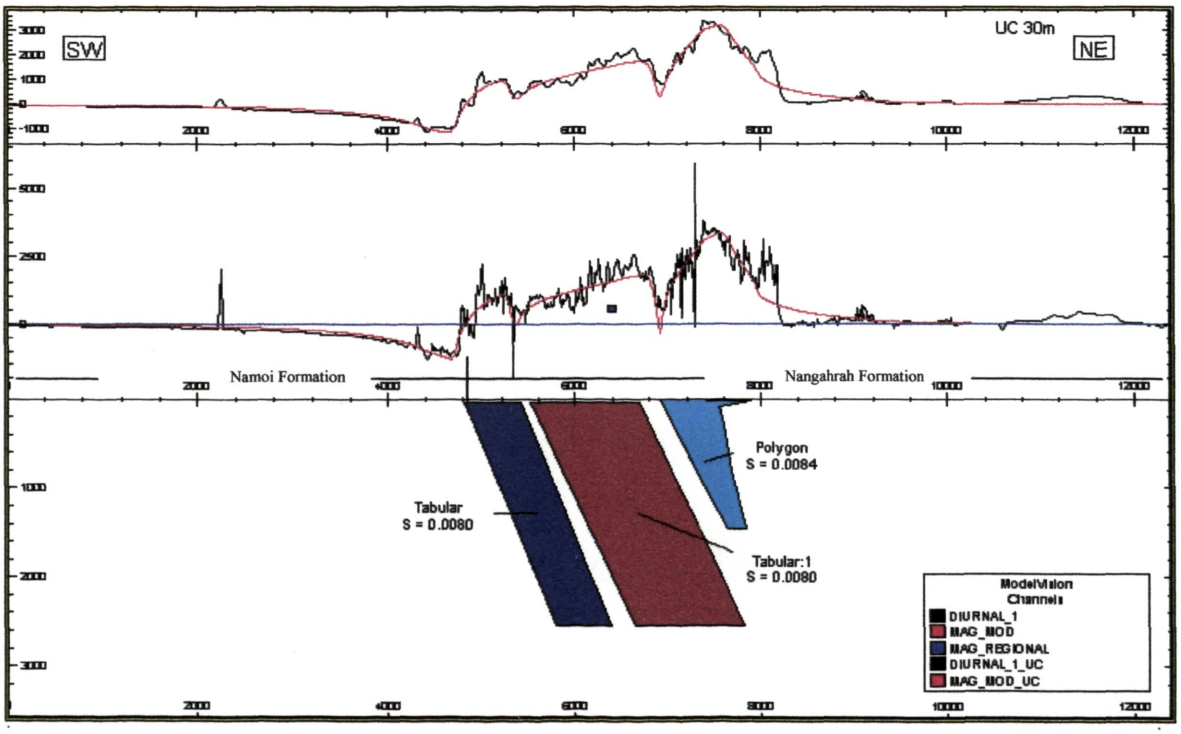

Figure 5.6a. 2-D magnetic model along the Barraba traverse (cross-section view). A complex structure was used to match the observed data. Both main tabular bodies dip steeply to east and have depth extent of 2.5 km and an azimuth of 340°, V/H =1. See Figure 4.8 for location of cross-section.

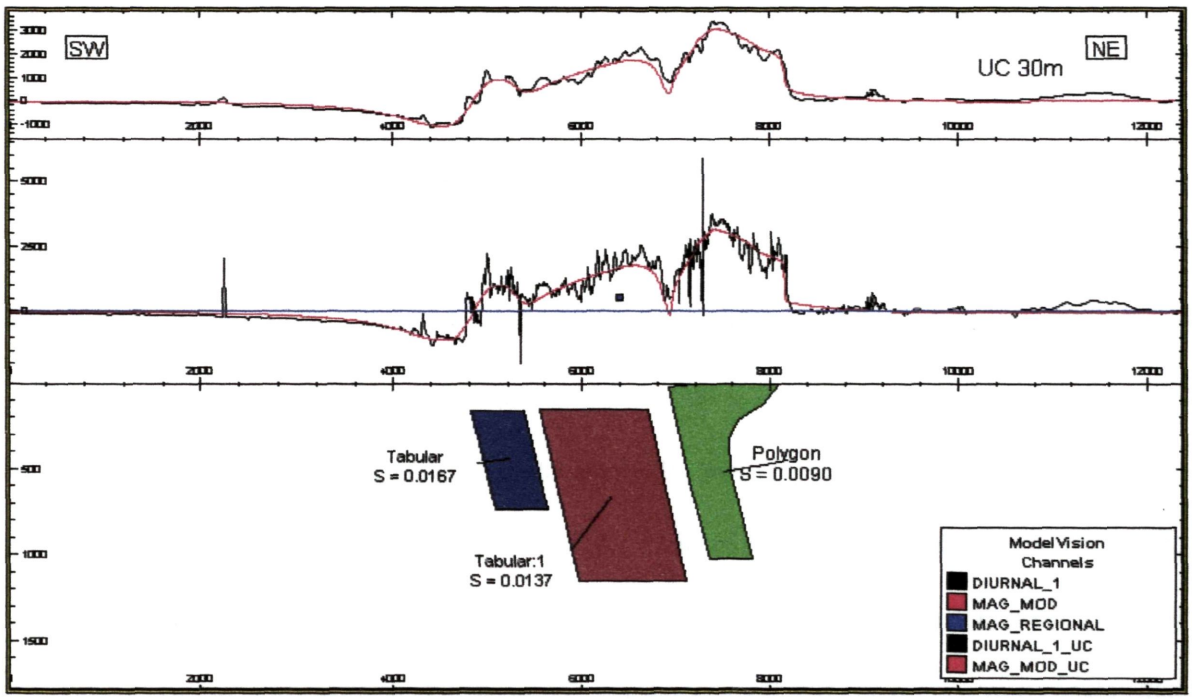

Figure 5.6b. 2-D magnetic model along the Barraba traverse (cross-section view). Two main tabular bodies with depth extent of less than 1km were used to match the observed data. The main tabular bodies required a very high susceptibility, and dip steeply to the east with an azimuth of 340°, V/H =1. See Figure 4.8 for location of cross-section.

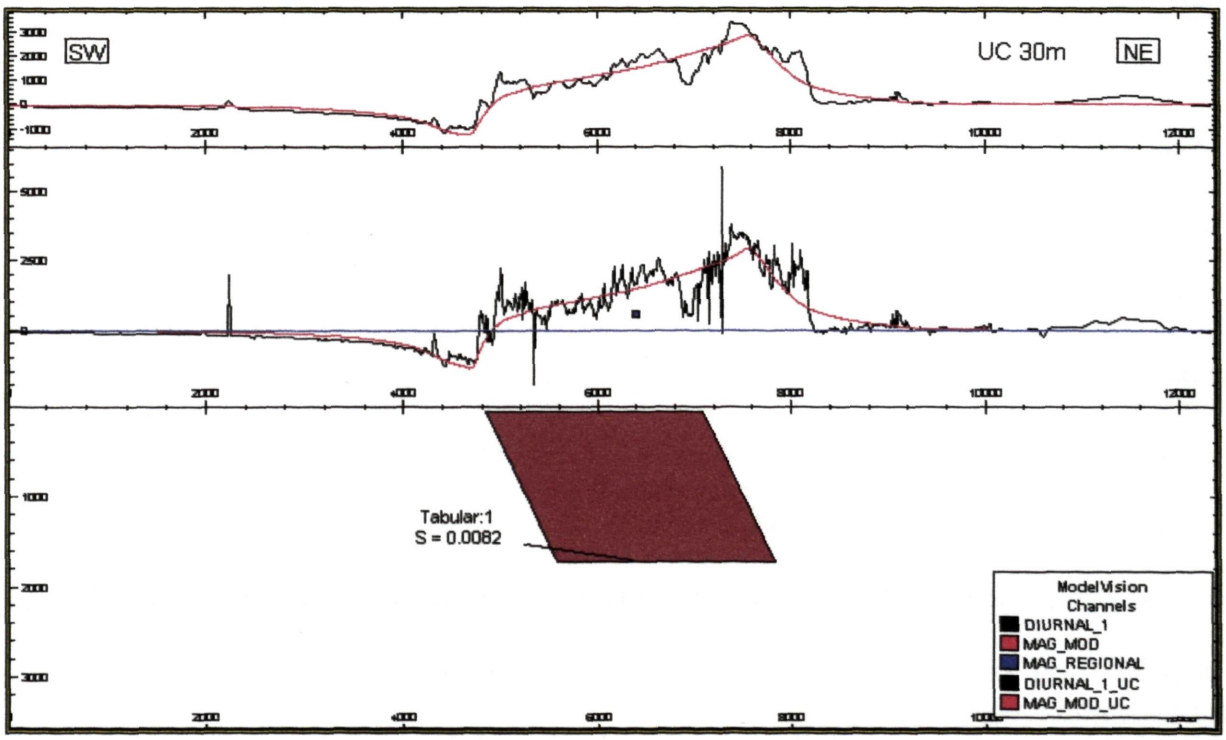

Figure 5.6c. 2-D magnetic model along the Barraba traverse (cross-section view). Single tabular body was used to produce a good fit to the observed data. The body dips to the east at 68°, with an azimuth of 340°. V/H =1. See Figure 4.8 for location of cross-section.

Line Nundle

The Nundle line was surveyed along the road to the east of the village of Nundle (Figure 4.8). Along the magnetic traverse, the Early Permian non-magnetic Andersons Flat Beds composed of sandstone and carbonaceous siltstone outcrops to the east of the Peel Fault, and Silver Gully Formation composed of sandstone, siltstone with minor metadolerite and metabasalt outcrops to the west (Gilligan and Brownlow, 1987; Ashley and Hartshorn, 1988). The data are shown in the Figure 5.7. The magnetic anomaly in Figure 5.7 has an amplitude of approximately 3000 nT with three major magnetic highs, the widest one of which is above an outcrop of serpentinite. No outcrops of serpentinite are known over the other two highs. The shape of the anomaly is the most complicated of all the magnetic transverses, and is better modelled by three large tabular bodies (Figure 5.7). The anomaly between 2400-3600 m corresponding to the serpentinite outcrop between 3200-3400 m along the surveyed line was modelled with an eastward dipping tabular body (Tabular4), which is wider by about 1000m than the actual outcrop of the serpentinite body, indicating the serpentinite is partly buried. A small tabular body two was introduced to the western edge of the Tabular body four to produce a good match, probably implying a heterogeneous susceptibility within the serpentinite. To the west of the tabular body four, an east-dipping tabular body zero was used to match the anomaly observed between 1100-1900m. No serpentinite outcrops on the surface above the modelled body. The outcrop is metadolerite and metabasalt of the Silver Gully Formation, producing a high magnetic response. To the east of the modelled tabular body four, the observed anomaly between 3900-4500m was modelled with an east-dipping tabular body (Tabular3). Two near surface small bodies were used to match the observed high frequency features to give a good fit to the data. The modelled bodies may represent buried serpentinite bodies beneath the anomaly between 3900-4500m. No serpentinite bodies outcrop in this area. However, the mapped Peel Fault corresponds roughly to the west edge of

the tabular 3 and some serpentinite rock pieces were found along the surveyed road in this area, suggesting its emplacement along the Peel Fault beneath the surface.

The model employing tabular bodies requires that they have different susceptibility values ranging from 3200-8400 × 10^{-6} cgs. The average value of the susceptibility of the collected serpentinite sample in this transverse is around 4500 × 10^{-6} cgs and is used for the widest tabular body, where serpentinite samples were collected, to fit the anomaly between 2400-3600 m. The depth extension and dip of the serpentinite bodies have not been assessed because of the complex shape of the anomaly. However, the depth extent of the serpentinite body depends strongly on the assumed magnetic susceptibility. Given the high values used in the best-fit model, there is little doubt these are minimum values.

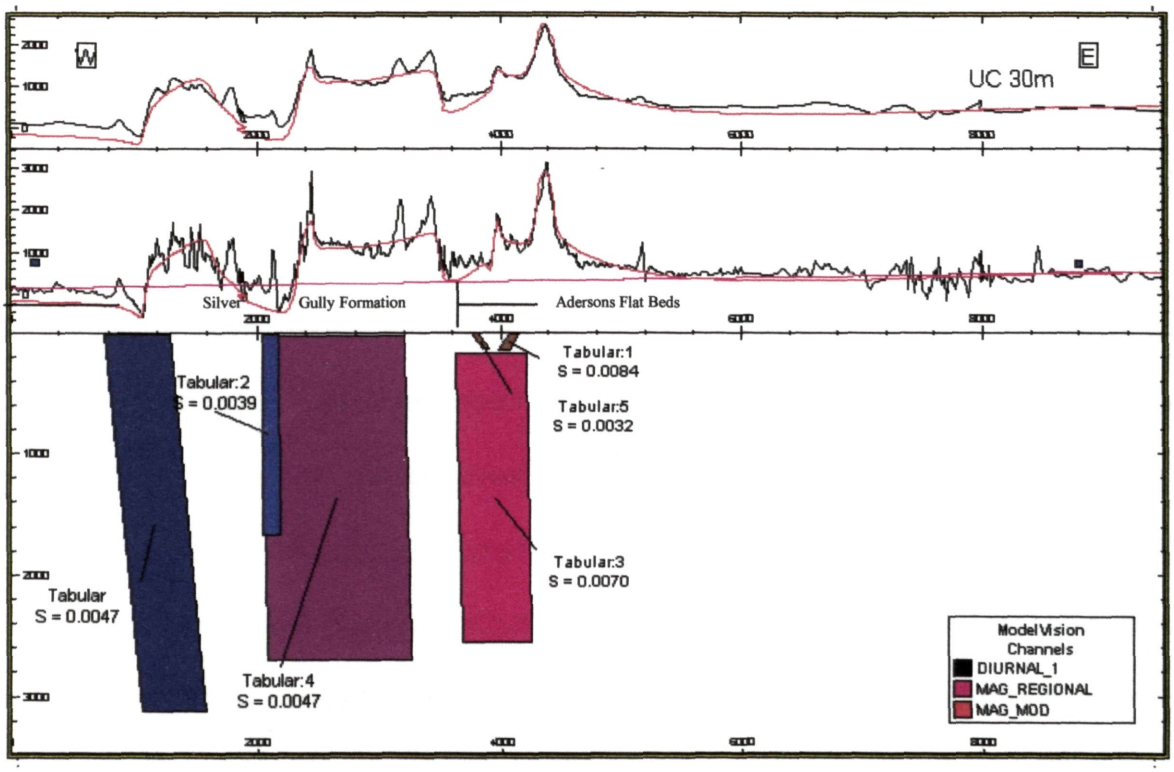

Figure 5.7. 2-D magnetic model along the Nundle traverse (cross-section view). A complex structure was used to match the observed data, V/H =1. See Figure 4.8 for location of cross-section.

5.4. Modelling result of aeromagnetic data

Modelling and interpretation of the regional magnetic data related to the Peel Fault offers another avenue to constrain the subsurface geometries of the serpentinite bodies. A series of magnetic profiles from Manilla in south to Bingara in north were extracted from regional aeromagnetic data consisting of the Peel and Peel South datasets released by Department of Mineral Resources, New South Wales under the Discovery 2000 geophysics project (Brown 2001, 2003). The magnetic profiles are perpendicular to the regional strike of the anomaly associated with the Peel Fault and were modelled. Magnetic interpretation of the dip of the serpentinite body requires that the Peel anomalies are separated as much as is possible from any adjacent anomaly or regional field. For every profile, a simple tabular body was used to fit the observed anomaly because there are no constraints on the subsurface structural information. Initially, the susceptibility, dip and thickness were adjusted to approximately match the anomaly, and then inversion of the model was undertaken to produce a best-fit model with susceptibility, thickness, distance, dip and depth set free. Susceptibility was limited to the range of the measured values for the inversion. The final "tweaking" to obtain best-fit models for the anomalies was done by trial and error. Figure 5.8a shows the bodies in plan view and Figure 5.8b shows a perspective view. The parameters of the modelled bodies are presented in Table 5.3, including the values of the dip, susceptibility, thickness, depth extension and azimuth etc. The azimuths of the modelled bodies were constrained in a range of 0-25° to conform to surface geological evidence (Brown et al., 1992). Most susceptibilities used for the modelled bodies approximately equal the average value of the measured susceptibility with a few exceptions requiring a higher susceptibility most likely due to a VRM contribution. The minimum depth extents of the serpentinite bodies are variable and most of them fall in to a range of 1-3 km. There is no independent information to constrain the dip value, but all traverses can be modelled as

steeply east-dipping bodies (Table 5.3), consistent with the geological observation with a few exceptions where the serpentinite bodies have a shallowly eastward dip of around 50° or less (Table 5.3). Serpentinite bodies dipping shallowly to the east include tabular 6, 9, 10, 11, 15, and 16. Bodies 15 and 16 occur near Upper Bingara, where ground magnetic traverse Tarakan was surveyed. Modelled serpentinite body 11 corresponds to the Woodsreef area, 9 and 10 correspond to Crown Mountain immediately south of Woodsreef, and 6 is located midway between Woodsreef and Manilla. The shallowly east-dipping modelled bodies generally correspond to the wider outcrops of the serpentinite with the exception of body 6. Body 6 is located in an area where the outcropping of serpentinite is very small, possibly reflecting a large blind serpentinite body under surface. In addition, these bodies also correspond to the intensively mined mineral deposits (gold and chromium) except for bodies 6 and 15. Modelled serpentinites 6 and 15 may suggest a future exploration area.

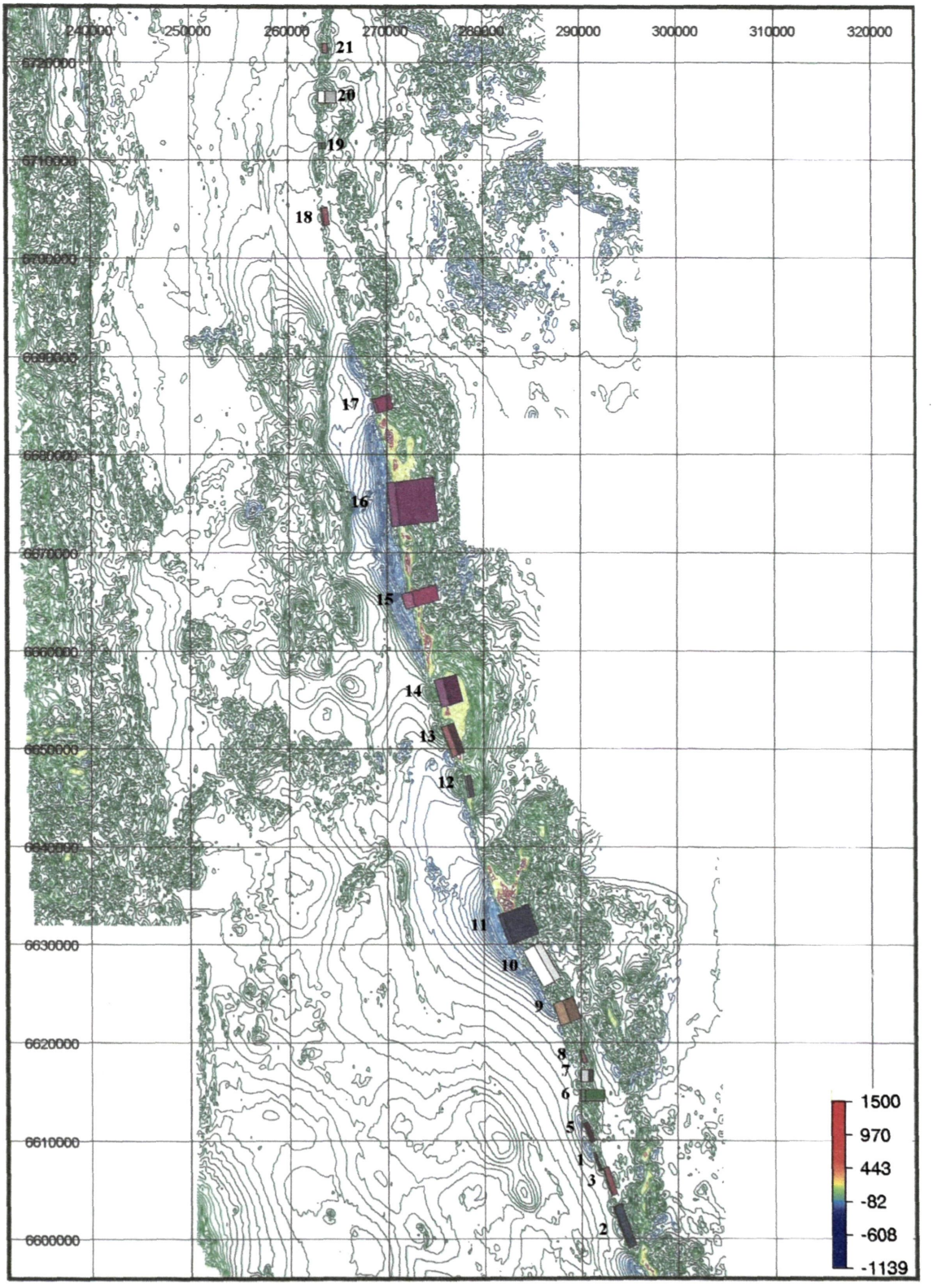

Figure 5.8a. Modelling in detail of the magnetic traverses across the Peel Fault extracted from the Peel aeromagnetic dataset. Traverses are normal the strike of the local magnetic anomalies. All traverses are modelled as simplified single tabular bodies to give an almost 3D view of the serpentinite bodies along the Peel Fault. The colour of tabular body is only used to mark the different modelled tabular bodies.

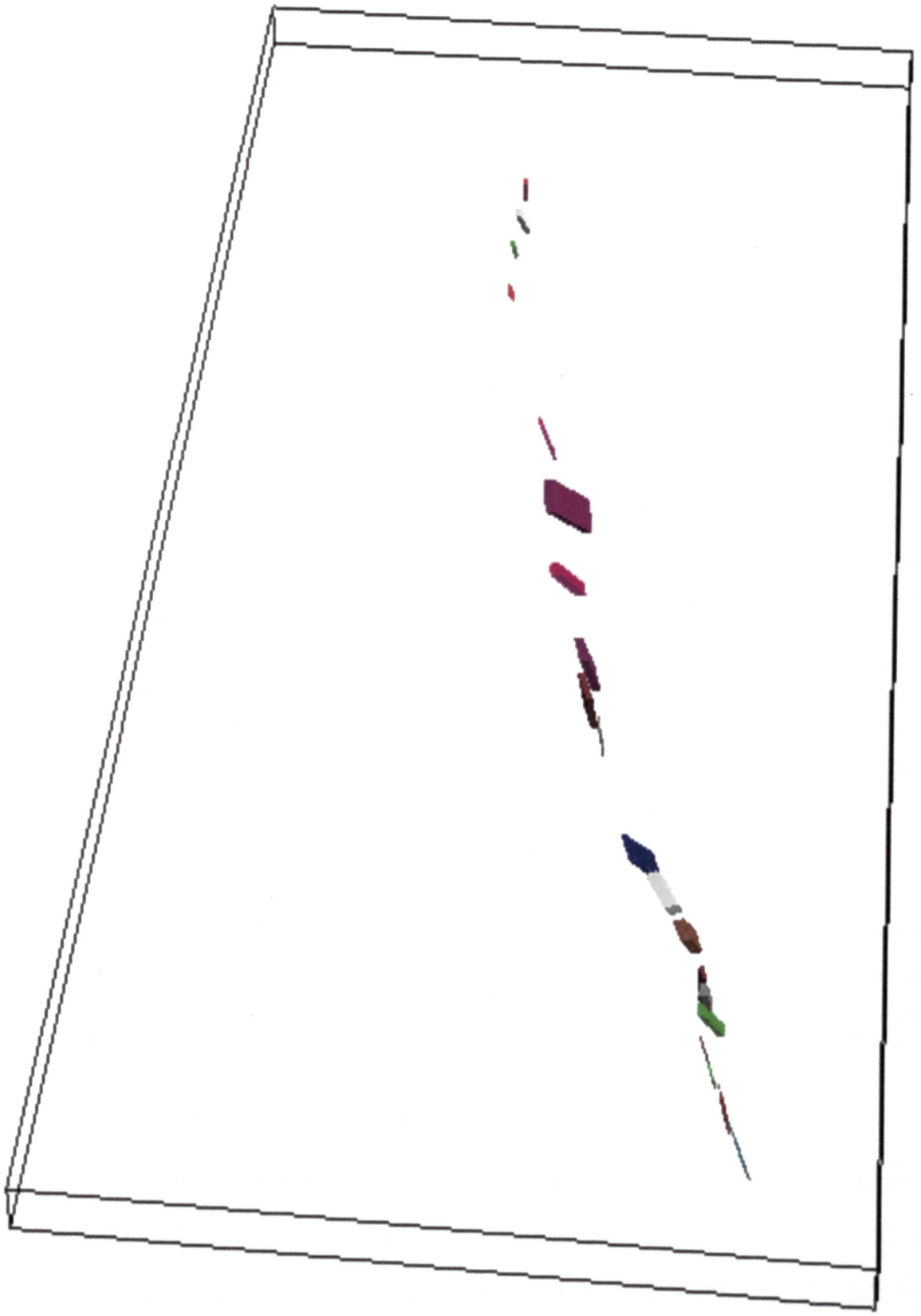

Figure 5.8b. Perspective view of Figure 5.8a.

Table 5.3 The parameters of the modelled tabular bodies

Body	Easting (AMG56)	Northing (AMG56)	Distance to surface(m)	Thickness (m)	Depth Extension(m)	Dip (°)	Strike Length(m)	Azimuth (°)	Susceptibility (cgs)
Tabular2	294020.6	6601130.5	65.2	81.5	2237.1	68.8	4565.1	-20.0	0.005940
Tabular3	292625.5	6605735.3	45.4	43.4	3615.1	80.8	2903.6	-18.0	0.002437
Tabular1	291565.3	6607813.1	104.5	128.3	756.6	79.3	1904.3	-20.0	0.004803
Tabular5	290610.3	6610767.9	121.2	116.6	1468.5	75.6	2123.6	-20.0	0.010652
Tabular6	290144.3	6614573.0	299.2	572.8	2003.7	45.0	1177.0	0.00	0.003081
Tabular7	290342.2	6616573.0	161.2	849.3	1769.6	75.4	1247.5	0.00	0.001692
Tabular 8	290187.1	6618573.0	240.8	404.9	3488.0	90.0	1277.4	-20.0	0.004116
Tabular 3	292625.5	6605735.3	45.4	43.4	3615.1	80.8	2903.6	-18.0	0.002437
Tabular 9	287954.3	6622997.9	233.1	1042.1	1629.4	54.3	2324.8	-20.0	0.001895
Tabular10	285638.5	6627772.0	689.6	1249.0	1019.7	52.5	4247.5	-30.0	0.004186
Tabular11	282201.3	6631545.6	108.8	404.6	2713.3	43.4	3247.5	-20.0	0.010695
Tabular12	278288.7	6646123.0	306.4	193.6	2605.5	79.8	2247.5	-10.0	0.023215
Tabular13	276520.4	6650761.7	313.5	652.4	3604.1	79.8	3247.5	-20.0	0.009933
Tabular14	275699.6	6655725.2	668.8	895.6	3633.7	69.1	2865.1	-15.0	0.014982
Tabular15	272198.5	6665140.0	170.4	1057.6	2627.2	45.0	1574.4	-15.0	0.008782
Tabular16	270632.7	6674902.5	66.7	846.4	2466.9	31.3	4483.4	-7.0	0.012160
Tabular17	268840.6	6684945.5	68.9	258.3	3792.2	67.9	1492.5	-15.1	0.004371
Tabular18	263503.9	6704221.1	22.2	133.3	821.7	55.7	1797.7	-8.0	0.000906
Tabular19	263316.9	6711441.0	70.0	275.7	1427.9	72.6	649.6	0.00	0.004097
Tabular20	263512.4	6716441.0	48.1	705.2	2043.6	60.5	1273.1	0.00	0.004382
Tabular21	263848.3	6721441.0	103.3	511.3	1989.9	88.8	997.6	0.00	0.003894

5.5. Sensitivity analysis of the susceptibility and depth

The inherent non-uniqueness of potential field modelling, i.e. a single anomaly may be produced by an infinite number of differing source bodies, requires input of rock property data and geological information to ensure that the results are as realistic as possible. These ambiguities could be reduced by more constraints, such as rock property data and available geological information from outcrops and drill-hole data (Dehler, 1991; McLean and Betts, 2003). The sensitivity analysis, to some extent, aids to better understand the ambiguities

associated with potential field modelling. Sensitivity analysis was undertaken to test how varying the rock property geometry of the serpentinites affects the geophysical response in the forward models.

The sensitivity analysis of the susceptibility uses the Glendu profile to illustrate the effects of systematically changing the susceptibility of the serpentinites (Figure 5.9a). The tabular body has a depth extent of 3 km, an eastward dip of 85°, a strike length of 3 km, azimuth of 335°, thickness of 800 m and a zero distance to the surface. The varying susceptibilities range from 1000 to 10000 × 10^{-6} cgs, and are consistent with the measured susceptibilities of serpentinites, falling into the 2000 to 9000 × 10^{-6} cgs range. The increase and decrease of the magnetic susceptibility is set to an order of 1000 × 10^{-6} cgs to get 10 results to evaluate the magnetic effect with a measured susceptibility range. The calculated magnetic effects of a tabular body with the variable susceptibility prove that the observed anomalies of around 2000 nT over the Peel fault require a susceptibility of at least 4-5000 × 10^{-6} CGS. This analysis indicates that the susceptibility of ~1000 × 10^{-6}cgs used by Ramsay and Stanley (1976) would not produce a magnetic anomaly of 2000 nT (Figure 2.5). There is no detailed explanation of how Ramsay and Stanley obtained their susceptibility values of the serpentinites. The reasons for obtaining a low susceptibility of the serpentinites probably include insufficient susceptibility readings and/or the method by which they measured the susceptibility of the serpentinites. Susceptibility values of samples (fresh) from this study, measured in laboratory are generally higher than that measured directly in field due to surface weathering of the rocks.

The geometries of the magnetized bodies are another factor affecting the modelled magnetic response. The geometrical sensitivity analysis of the Glendu profile was conducted with a constant rock property. The magnetic body has a susceptibility of 10000 × 10^{-6}cgs, a thickness of 800 m, an eastward dip of 85 °, an azimuth of 335°, a strike length of 3 km and a

zero distance to the surface. The depth of the tabular body is adjusted to assess how this affects calculated magnetic response (Figure 5.9b). I have focused on defining the minimum depth to the base of the serpentinite body to see if the Peel Fault could be truncated by a shallow (~1 km) major west-dipping structure as proposed by Korsch et al (1993). The calculated magnetic effects of a tabular body with the variable depth show the calculated values at 3 km, 4 km, and 5km are very similar (Figure 5.9b), indicating that only the minimum depth of the extension of the depth to the base of the serpentinite can be concluded by the modelling.

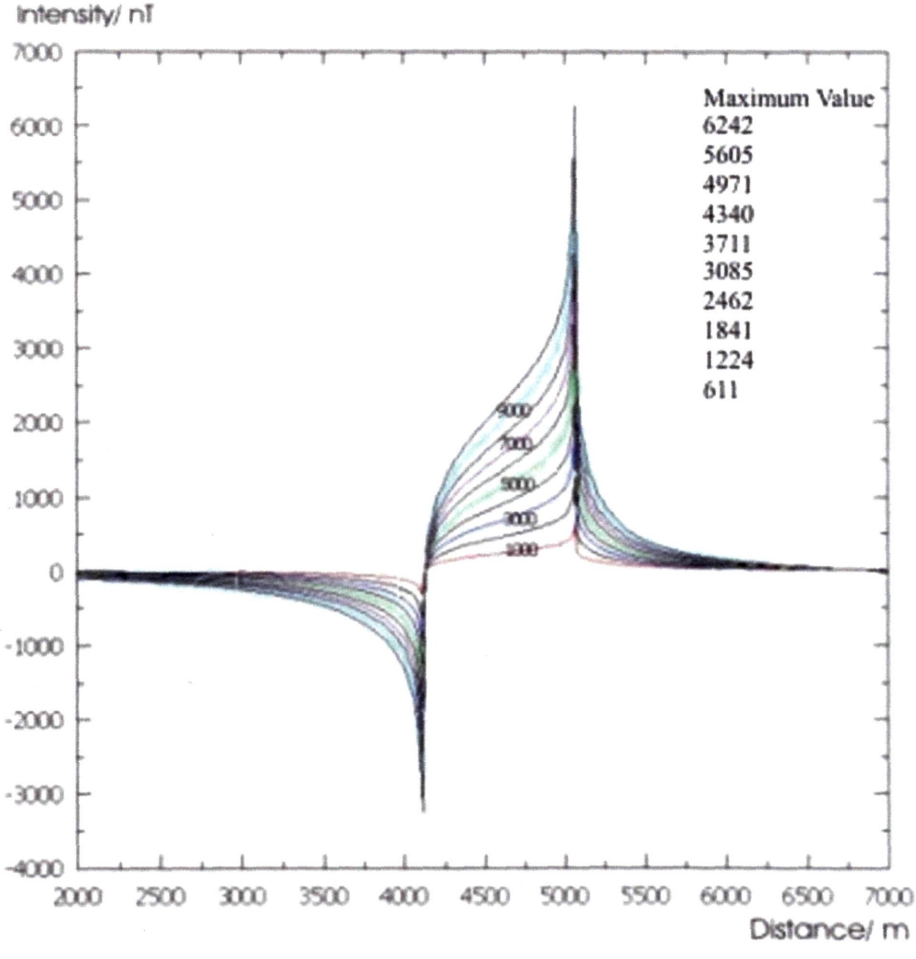

Figure 5.9a. The calculated magnetic effects of a tabular body with the variable susceptibility. Numbers across the curves represent susceptibility values ($\times 10^{-6}$ CGS) used to calculate magnetic responses of the given tabular body. An anomaly of around 2000 nT requires a susceptibility of at least 4-5000 $\times 10^{-6}$ CGS.

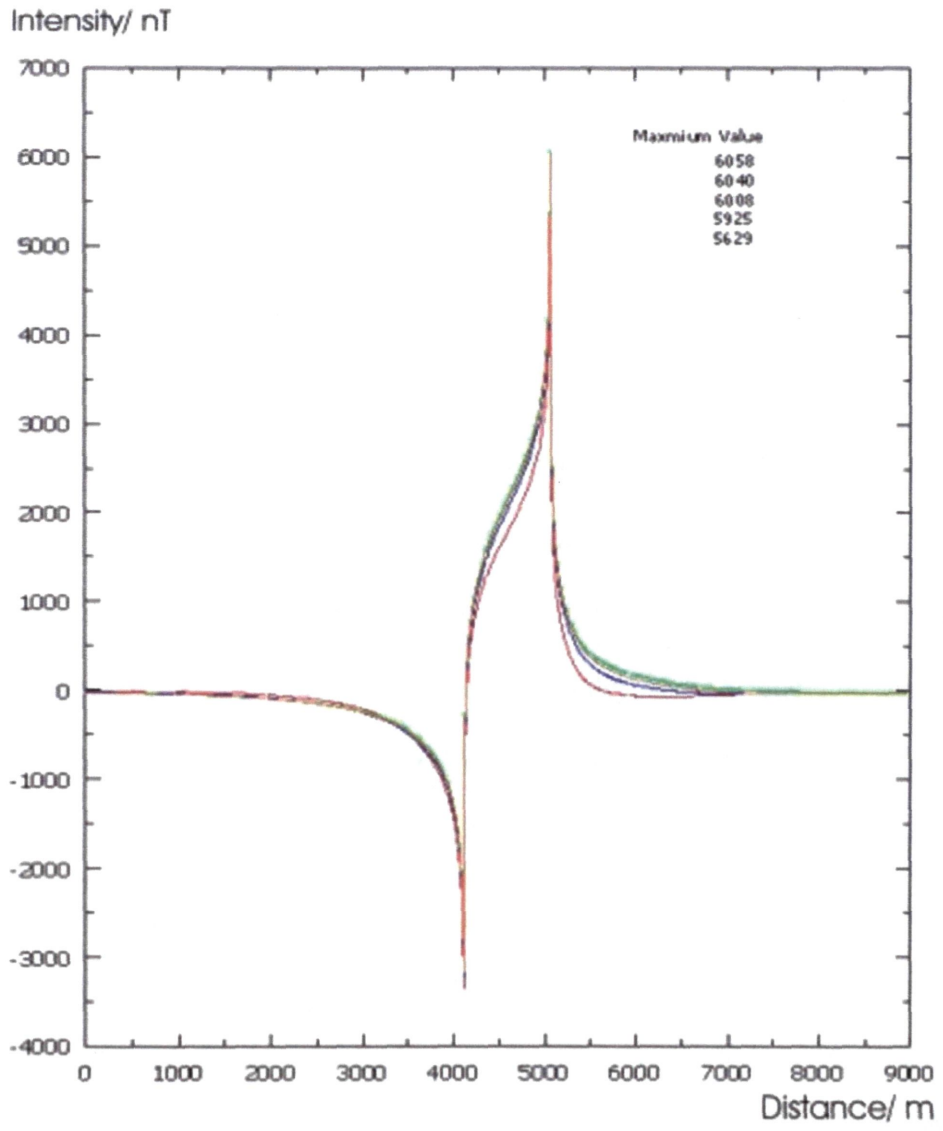

Figure 5.9b. The calculated magnetic effects of a given tabular body with the variable depth. The calculated values at 3 km, 4 km, and 5km are very similar. The values in the top right corner show the maximum amplitude from 5 km to 1 km.

5.6 Discussion of the modelling results

This study models five ground magnetic transverses across the Peel Fault, Great Serpentinite Belt of NSW from Nundle in the south to Bingara in the north. All transverses were modelled to get a best fit for the observed magnetic anomalies with single steeply eastward dipping tabular bodies or multiple bodies of serpentinite. In case of the Manilla and Glendhu profiles, steep west-dipping tabular bodies can also produce a good fit to the

observed anomaly. The steep west dipping tabular body for Glendhu magnetic anomaly has a very steep dip of 88°, almost vertical, which is not very different with the eastward dip of 85° of the modelled body producing the best fit for the anomaly. A tabular serpentinite body with both a westward dip of 64° and eastward dip of 86° produced a good fit for the Manilla magnetic anomaly. No geological evidence is available to support or deny one of two assumptions due to the lack of the outcrop of the serpentinites within the area surveyed.

Modelling of all ground magnetic data show that the Peel Fault can be modeled as a relatively steeply dipping fault to the east (with one exception), which supports the geological observations in the study area (e.g. Benson, 1913, 1915; Crook, 1963; Rod, 1974). The exception is Tarakan profile, where the serpentinite body is best modelled as a relatively shallowly eastward dipping body (50°). Modelling of the extracted transverses from the Peel dataset indicates that most serpentinite bodies have a steep eastward dip, which is consistent with the results of modelling of the ground magnetic data and the published outcrop-structural data. The serpentinite bodies dipping shallowly to the east generally correspond to the wider outcrops of serpentinite. These new results are consistent with previous magnetic modelling by Ramsay and Stanley (1976), later Woods (1988), Edwards (1996) and Carter (2003), all of which indicated similar results that the Peel Fault dips steeply to east assuming that the serpentinite was emplaced along the Peel Fault.

The ground magnetic modelling of this survey has produced a variable minimum depth extent of the serpentinite body from 800m to 3 km. At Tarakan near Bingara, the modelled eastward tabular body that produced the best fit for the observed anomaly has a depth extent of minimum 1300 m with an average susceptibility of 3903×10^{-6} CGS. The depth extension of less than 1 km such as 800 m was also modelled with a slightly higher susceptibility of around 4900×10^{-6} CGS, which is reasonable, in consideration of the possible minor surface alteration of some samples and the non-homogeneity of the susceptibility. At Manilla,

modelling of the magnetic data collected near the Seismic Line BMR G91-01 indicates that an eastward tabular body with a depth extension of 2.5 km produced the best fit, which is inconsistent with the interpretation of the seismic data by Korsch et al (1993a, b, 1997). However in case of the introduction of small westward dipping body, the depth of the modelled bodies could be reduced to less than 1 km. No surface geological information indicates this small body exists, which may be a subsurface small mafic sill similar to that reported 25 km south in Attunga (Leitch, 1979). The modelled tabular bodies for the rest of magnetic data collected near Barraba, Glendhu and Nundle, require a depth extension of at least 2.5 km or deeper.

The minimum depth extent of the serpentinites inferred in this study differs from the work of Ramsay and Stanley (1976), in which deeper serpentinite bodies of 5 km were proposed. The sensitivity analysis of susceptibility, however, indicates that the susceptibility of ~1000 × 10^{-6} CGS used by Ramsay and Stanley (1976) would not produce the observed magnetic anomalies with magnetic amplitude of 2000 nT. The work of Edwards (1996) and Carter (2002) ruled out the possibility of a minimum depth of less than 1 km for the serpentinite body at Kootingal and that in the Cobbadah area. A minimum depth of 800 m to the base of serpentinite obtained at Tarakan is consistent with interpretation of Woods (1988).

The modelling of the transverses extracted from the aeromagnetic dataset shows that most of the modelled bodies from the south near Tamworth to the north near Warialda dip to the east, and this is consistent with the conclusion obtained from the ground magnetic model.

5.7 Tectonic Significance of the Great Serpentinite Belt of NSW

The mechanism of emplacement of not only the Great Serpentinite Belt of NSW but also alpine peridotite belts elsewhere has been debated for many years. The generally accepted emplacement models have varied over the years according to the current geological paradigm

(e.g. Moores, 1982; Pearce, 2003). Early studies interpreted serpentinite in a continental environment as plutonic intrusions into folded geosynclinal sedimentary rocks (e.g. Benson, 1926). The plate tectonic revolution shed new light on the emplacement of ophiolites and soon after serpentinite bodies were interpreted as fragments of fossil oceanic lithosphere that have been thrust over or "obducted" into continental margins or platform at consuming plate boundaries or as the incorporation of a relatively undeformed ophiolite slab in a subduction complex (Coleman, 1971; Moores, 1982). With the increasing awareness of the diversity of ophiolite, ophiolite was reported to have the structures or inferred structures of oceanic crust, yet a geochemical composition which indicates that they formed not at mid-ocean ridges but at spreading centres near subduction zones (Pearce, 2003). With the discovery of serpentinite seamounts in the forearc regions of modern subduction zones, most ophiolites are seen as forming above subduction zones, and grouped as the class known as supra-subduction zone ophiolites (Bloomer et al., 1995; Pearce, 2003).

There are several models of the emplacement of the serpentinite in the SNEFB. W. N. Benson in a classic series of papers published early last century (Benson 1913, 1926), described the Great Serpentinite Belt of NSW and argued that the serpentinite bodies were emplaced as intrusions. Since the acceptance of the plate tectonic model about 30 years ago, serpentinite bodies have been considered to be part of "a dismembered ophiolite" (e.g. Crook and Felton, 1975). There has been a consensus that the serpentinite is part of an ophiolite sequence representing ancient oceanic crust and upper mantle material, and must have been tectonically emplaced (Crook and Felton, 1975; Pooley, 1979; Cross, 1983; Rogers, 1986; Yang et al, 1997). A few emplacement mechanisms of the serpentinite were suggested, including "scraped", "obduction", "seamount", and "mantle wedge".

The classic obduction model was proposed by Scheibner and Glen (1972), who suggested that the serpentinite represents slices of ocean floor on which the Woolomin flysch

wedge was deposited, and that the ocean floor was formed during the Middle and Upper Silurian. Scheibner (1999), with a modern analogue of the Papua-New Guinea Ultra Mafic Belt, further suggested that young, only a few kilometres thick oceanic lithosphere forming basement to a volcanic island arc could be obducted along with arc, and that the serpentinite in the accretionary prism of New England Fold Belt was formed by obduction of thin oceanic lithosphere during tectonic compression. However, the details of the emplacement mechanism of serpentinite onto the forearc sediments are still controversial.

The "scraped" model was suggested by Dilek (2003), who summarised the structural architecture, chemical fingerprints, and evolutionary paths of a variety of ophiolite preserved on land, and suggested that the Great Serpentinite Belt has the same tectonic origin as the Franciscan Ophiolite that outcrops along the west coast of North America. Both ophiolites are spatially associated with accretionary complexes and are tectonically intercalated with melanges and high-pressure metamorphic rocks characteristic of a subduction zone. Dilek (2003) suggested that these serpentinites are tectonic slices of oceanic rocks scraped off from downgoing plates, and are tectonically imbricated. They become progressively younger in age structurally down-section within the subduction-accretionary complexes as observed in the Tablelands complex, where the oldest Woolomin association locates immediately east of the Peel Fault, and to the east the Sandon association and Nambucca association.

Cawood (1982) suggested that the Peel Fault may have had a long and complex history, and its movement changed from essentially convergent to dominantly strike-slip during the Late Carboniferous to Early Permian. The fault provided suitable pathways for the cold-solid diapiric rise of mantle-derived serpentinite. Aitchison and Ireland (1995) proposed a similar model for the emplacement of the serpentinite. They suggested that the serpentinite represents portions of a Cambrian intra-Oceanic arc rift sequence over which the Tamworth belt and part of the Tablelands Complex may have been thrust westwards as a series of thin-skinned nappes

over older basement during the process of their accretion to the margin of Gondwana. The serpentinite bodies were later exposed as a result of extensional normal faulting related to latest Carboniferous to Early Permian strike-slip faulting (Corbett, 1976; Offler and Williams, 1987), which has been proposed as a mechanism that played a part in the formation of the S-Type Bundarra Plutonic Suite and the possible diapiric rise of serpentinite-matrix melange along the Peel Fault. A 530±6 Ma $^{206}Pb/^{238}U$ zircon date on an included block of plagiogranite from a serpentinite body near Upper Bingara in the northern part of the serpentinite belt (Aitchison et al, 1992a) and middle Ordovician (K-Ar ages of 465-480 Ma) high PT metamorphic rocks from blocks in the serpentinite melange near Glenrock station and Pigna Barney River in the southern part of the serpentinite belt (Fukui et al., 1995) constrain the maximum age of 530 Ma.

Cao (1994) proposed a model for the emplacement of the serpentinite on the basis of the analysis of the structures in the serpentinite bodies near Manilla. He suggested that the Peel Fault started with a precursor within the basement of the forearc basin, and has undergone five stages of movement. Initially a decollement of a forearc basin to a high-angle reverse fault, then a sinistral transpressional fault, and an extensional fault and finally went back to being a thrust.

An alternative interpretation of the emplacement of the serpentinite is that the serpentinite and its associates were brought to the surface from a Lachlan Fold Belt source (Korsch et al., 1993a, 1997) up a moderate west-dipping structure imaged on a deep seismic profile across the New England Fold Belt by Geosciences Australia (Korsch et al., 1993a, 1997). Recent research suggests that serpentinite would emplace along a vertical structure in supra subduction zone (Frey, 1995; Maekawa et al., 1995). No evidence indicates that the serpentinite could emplace on a structure dipping at an angle less than 30°.

5.8 Tectonic Emplacement of the Serpentinite

Most existing models for the Palaeozoic tectonic development of the New England Fold Belt involve progressive accretion of increasingly younger rocks to the cratonic margin of eastern Gondwana (e.g. Leitch, 1975; Korsch, 1977; Cawood, 1982; Murray et al, 1987). The emplacement of the Great Serpentinite Belt along the Peel Fault forms a key element in unravelling the Palaeozoic tectonic history of the NEFB. There are many suggestions or interpretations about the emplacement of the serpentinite as discussed above. However, only those models that result in serpentinite being emplaced along steep faults are supported by this study. Except for the geometry of the serpentinite body, a model for the emplacement of the serpentinite also needs to reconcile the facts that the serpentinite is perhaps the oldest rock (Aitchison et al, 1992a) preserved in the New England Fold Belt. Eclogite blocks in serpentinite have a crystallization temperature of between 290-600°C associated with minimum pressures of 0.7-1.2 Gpa near Attunga (Shaw and Flood, 1974) and 410-530°C with pressures of 1.0-1.4 Gpa Near Gleneden south-east of Nundle (Allan and Leitch, 1992). In the following paragraphs, a preferred model for the emplacement of the serpentinite will be proposed on the basis of the results from this study, incorporating with the previous published data on the age and geochemical features of the serpentinite.

5.8.1 Scraped Model of Emplacement

A preferred model proposed here, which is reasonably consistent with all of the available data, is that the serpentinite represents remnants of an oceanic upper mantle scraped off from a downgoing plate during the Silurian (?)-Carboniferous episode of plate convergence. The tectonically sliced ophiolite (Great Serpentinite Belt) initially dipped to west as observed in modern accretionary prism of the Aleutian arc system (Von Huene and Scholl, 1991), and then its dip became more vertical and finally most serpentinite dipped steeply to east as

observed in Great Serpentinite Belt due to the intense contraction with the continuation of the subduction. The history of the formation and emplacement of the serpentinite could be also divided into five stages as proposed by Cao (1994) but with different features.

Early Cambrian-Silurian (?) stage: The serpentinite (old oceanic crust 530 Ma) may have been generated at the mid ocean ridge east of Gondwana and received Cambrian (?)-Silurian (?) abyssal sediments. This interpretation is supported by the recognition that the serpentinite along the Peel Fault are dismembered ophiolitic rock representing oceanic crust (Crook and Felton 1975; Pooley, 1979; Cross, 1983; Rogers, 1986) with a 530±6 Ma $^{206}Pb/^{238}U$ dating on an included block of plagiogranite from a serpentinite body near Upper Bingara in the northern part of the serpentinite belt (Aitchison et al, 1992a). Yang and Seccombe (1997) analysed the geochemical features of the mafic and ultramafic complexes of the northern Great Serpentinite Belt from Upper Bingara to Paling Yard, and further suggested that the serpentinite of the northern Great Serpentinite Belt has a feature of single-stage melting, and probably represents oceanic crust formed in an open oceanic basin.

Anytime within this stage, a westward subduction started along a transform fault (a precursor of the Peel Fault?), formed anywhere between the eastern margin of Gondwana and the mid ocean ridge. The tectonic slices scraped from the oceanic rocks of the downgoing plate accreted to the front of the arc related to the subduction, and formed the accretionary wedge (Tablelands Complex) of the westward subduction zone. The dismembered ophiolite (Great Serpentinite Belt) tectonically was accreted to the east of the forearc basin deposition (Tamworth Belt) along the Peel Fault. The absence of deep marine sediments between the serpentinite and the Tamworth Belt probably indicate that the subduction started shortly after the formation of the downgoing plate. The serpentinite along the Peel Fault was part of the scraped tectonic slices, which were bounded by steep (west-dipping) faults to the west at this stage.

Silurian onward: With the continuation of the tectonic accretion, slices scraped from the underthrust plate early in the development of the wedge became steeper and the dip of the serpentinite associated with the Peel Fault remained steep or partly over-turned. The rocks of the accretionary wedge (Tablelands Complex) were structurally imbricated and have a series of steeply inclined fault, which separated different accretionary units such as the Woolomin and Sandon associations (e.g. Korsch, 1977). Progressively younger volcaniclastic flysch deposits, locally incorporating scraped-off ocean floor sediments and volcanics, accumulated at the front arc, and represented by the Late Silurian-Middle Devonian Woolomin Beds in west, through to the Late Devonian-Early Carboniferous Texas Sandon beds, to the Early Permian Nambucca beds in the east (e.g. Leitch, 1974, 1982; Korsch, 1977; Murray, 1997).

Late Carboniferous to earliest Permian stage: The Peel Fault region was under an extensional environment after westward subduction ceased or during retreat of the westward subduction (Korsch, 1982; Leitch, 1988; Cao, 1994; Jenkins et al., 2002), which was characterised by extensional basin formation (Barnard Basin) developed near and along the Peel Fault (Allan and Leitch, 1990). The wrench movement associated with the relaxation of subduction was observed during this period (e.g. Cao, 1994). The emplacement of the S-type Hillgrove and Bundara Supersuite of New England Batholith and rifting of the early Sydney-Gunnedah Basin could be related to this extension.

Mid-Permian to Triassic stage: Orogenic contraction (Hunter and Bowen Orogen) caused compression of the complex basin in the New England region and also deformation of older accretionary wedge rocks. The forearc sediments are folded and displaced by thrust faulting along the Hunter-Mooki and Kelvin Faults, the west margin of the Tamworth Belt (e.g. Liang, 1991; Woodward, 1995; Korsch et al., 1997). Many of the sub-horizontal detachments found under the Tamworth Belt imaged by the deep seismic profile recorded by GA (e.g. Korsch et al., 1993a, 1997; Glen et al., 1993) probably occurred at this time

(Scheibner, 1993; Cao, 1994; Korsch et al, 1993a, 1997). The Peel Fault was finally tilted to the present eastward dipping fault.

Although the "scraped" model could explain the available data so far, it is worth noting that the first-stage melting feature of the mafic and ultramafic complexes of the northern Great Serpentinite Belt suggested by Yang and Seccombe (1997) is not supported by the work of Cross (1983) and Aitchison et al (1994), who both proposed a highly refractory mantle source. Cross (1983) identified the low-Ti refractory nature of the Pigna Barney serpentinite in the southern portion of the Great Serpentinite Belt, indicating a supra-subduction zone setting within a primitive intraoceanic arc or incipient basin. Aitchison et al (1994) published the value of Cr/Y for the basalts of the Great Serpentinite Belt, which are similar to ophiolites and other rocks generated elsewhere in a supra-subduction zone setting. Given a serpentinite with island arc origin, an alternative tectonic model for the emplacement of the Great Serpentinite Belt could be proposed.

5.8.2 Alternative Tectonic Model

The emplacement of the serpentinite along the Peel fault could be the result of serpentinite diapirs rising similar to the serpentinite bodies recently described in the Supra-Subduction-Zone setting during the initiation of the westward subduction on the currently active forearc part of the Izu-Bonin-Mariana arc system, and exposed as serpentine seamounts generated in the forearc regions of the modern arc system. These are very similar to some serpentine bodies found as "sedimentary serpentinite" deposits in accreted fragments of former convergent margins on land (Fryer, 1995). The seamounts to a depth of 15-20 km in the active convergent margin are composed mainly of unconsolidated flows of serpentine muds containing clasts of serpentinized mantle peridotite, and located spatially 50-100 km away from the trench axis (Figure 5.10a) (Hussong and Fryer, 1985; Fryer et al, 1985; Fryer

et al, 1999, 2000). Seamounts are common on the outer half of the Mariana forearc (Fryer, 1995). Fryer (1995) suggested that within the active subduction zone, the mantle peridotite above the subducting slab has reacted with water to form serpentinite, and the resulting low-density serpentinite has risen to form a zone of seamounts (Figure 5.10b). The study of the blueschist-facies metamorphism in the Mariana forearc also indicates that the blueschist-facies rocks formed at depths and have been brought to the seafloor by upwelling serpentinite materials along fault planes parallelling the trench (Maekawa et al., 1995). Fryer et al (1995) suggested that formation and emplacement of the serpentine seamounts related to mud volcanoes composed of unconsolidated serpentine flows. In any case, serpentinite materials, which come up from depths to the seafloor, must have entrained oceanic mantle and crustal materials situated within the pathway to the surface (Maekawa et al., 1995). Analogous serpentinite bodies in land to those of the Mariana and Izu-Bonin seamounts occur at New Idria and Wilbur Springs, California (Fryer, 1995).

For the Great Serpentinite Belt along the Peel Fault, Cross (1983) concluded that the low-Ti basalts and norite of the southern portion of the Great Serpentinite Belt were crystallised from refactory melts generated from a depleted mantle source, indicating an island-arc ophiolite related to Palaeozoic supra subduction. Aitchison et al (1994) further supported this conclusion on the basis of the value of Cr/Y for basalts from the serpentinite in Pigna Barney region of the southern part of the Great Serpentinite Belt. The inclusions of rocks from different structural levels within the serpentinite in New England Fold Belt have a crystallization temperatures of between 290-600°C associated with minimum pressures of 0.7-1.2 Gpa near Attunga (Shaw and Flood, 1974) and 410-530°C with pressures of 1.0-1.4 Gpa Near Gleneden south-east of Nundle (Allan and Leitch, 1992), indicating the same origin as proposed by Maekawa et al (1995). The gravity and magnetic modelling in this study showed that most of the serpentinite bodies steeply dip to east, and are consistent with an

emplacement of the serpentinite along a subvertical pathway. The emplacement of the serpentinite during the initial stage of Palaeozoic subduction reconciled the 530±6 Ma $^{206}Pb/^{238}U$ dating on an included block of plagiogranite from a serpentinite body near Upper Bingara in the northern part of the serpentinite belt (Aitchison et al, 1992a) and high PT metamorphic rock of the K-Ar ages of 465-480 Ma exposed in Glenrock Station and Pigna Barney (Fukui et al., 1995). The differences between the ages by Aitchison et al (1992a) and Fukui et al (1995) showing plate convergence continuation of initial stage for at least 60 Ma (Fukui et al., 1995). Fukui et al (1995), on the view of the history of Izu-Bonin active plate boundaries, suggested that Early Cambrian serpentinite may have been generated at the onset of convergent plate activity as reported from modern analogy (Stern and Bloomer, 1992), and convergence continued for at least 60 Ma and formed middle Ordovician high PT metamorphics near Glenrock Station and Pigna Barney.

The emplacement of the serpentinite along the Peel Fault in a supra subduction zone setting could be described as follows.

Pre-Cambrian. A transform fault formed in the ocean floor east of Gondwana.

Early Cambrian-Middle Ordovician (?). The oceanic transform fault was converted into a subduction zone and westward subduction started. Serpentinite diapirs rose from the mantle wedge to the seafloor (Maekawa et al., 1995) to form a zone of seamounts in the outer ridge of the forearc. The included rock blocks may derive from the subducted slab or from the pathway walls within any part of the overriding plate (Maekawa et al., 1995; Fryer et al., 2000).

Onward. The tectonic slices scraped from the oceanic rocks of the downgoing plate and accreted to the front of the arc and formed the accretionary wedge of the westward subduction zone until the Early Permian as described in above model. The retreat and advancing of the downgoing plate during this period led to the shift of the volcanic chain (e.g. Cawood and

Flood, 1989; Liang, 1989). From the Late Carboniferous to the Early Permian this model has same tectonic process as discussed in the "scraped" model earlier in this chapter.

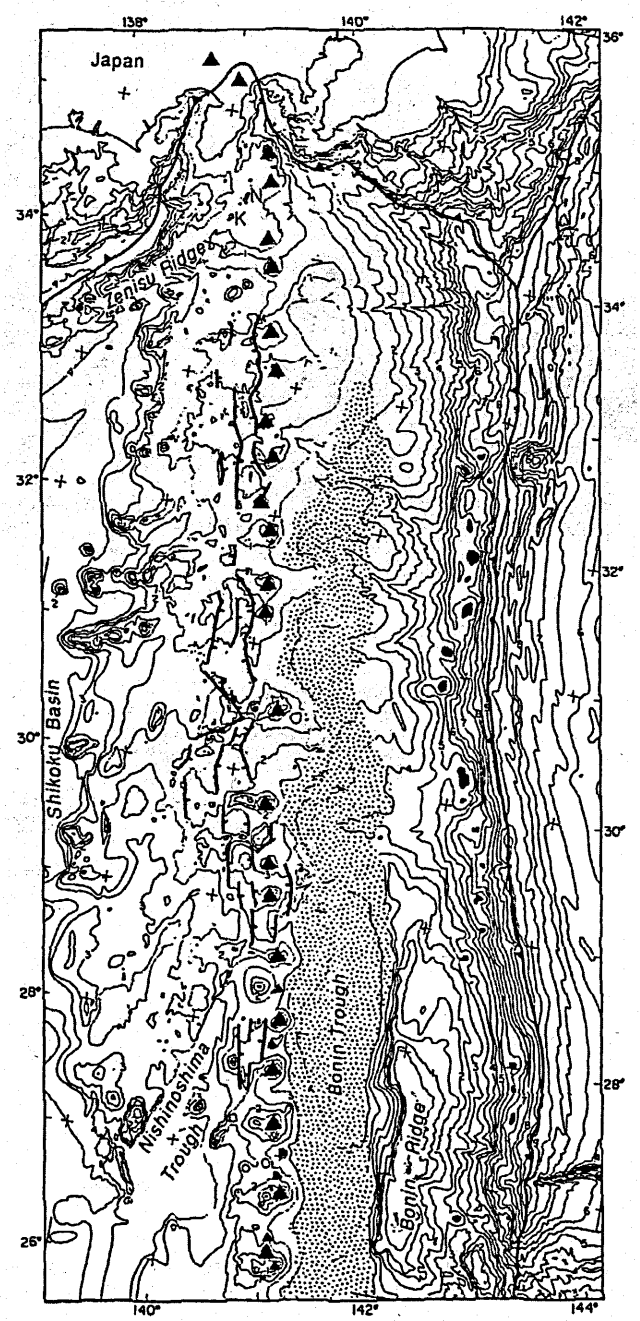

Figure 5.10a Bathymetry of the Izu-Bonin forearc showing the major structural elements of the convergent margin. Solid lines with triangles indicate trench axes. Solid lines with hatchures indicated major bounding faults of rift graben. Shaded area indicates forearc rift basin. Triangles indicate active volcanoes and irregular-shaped solid markings just west of the trench indicate forearc serpentinite seamount locations. (After Fryer, 1995)

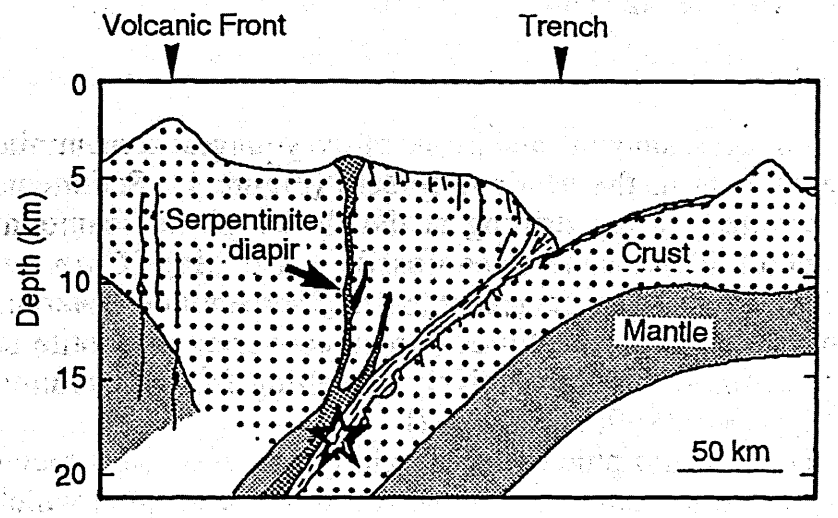

Figure 5.10b Cross-section showing the tectonic framework of the Mariana arc-trench system (After Maekawa et al., 1995)

CHAPTER SIX: MODELLING AND INTERPRETATION OF THE MAGNETIC DATA OVER THE MOOKI FAULT

6.1. Introduction

The Mooki Fault, along which the Tamworth Belt has been thrust westward over the eastern margin of the Permian Sydney-Gunnedah Basin, marks the western edge of the Tamworth Belt. Although both the deep seismic (Korsch et al, 1993a, b, 1997) and magnetic surveys (Ramsay and Stanley, 1976) over the fault indicate that the Mooki Fault has a dip of 25° to the east, there is no satisfactory interpretation of geophysical data to constrain the subsurface geometry for the entire Mooki Fault on a regional scale.

The interpretation of two ground magnetic surveys and three lines extracted from the Discovery 2000 aeromagnetic data (Brown, 2001, 2003) covering the study area have been done from Quirindi in the south to Tulcumba in the north (Figure 6.1a, b). The prominent magnetic anomalies over the Mooki Fault can be modelled to obtain the subsurface geometry of the Mooki Fault. In this chapter, on the basis of the ground magnetic data, several 2.5 dimensional magnetic models have been developed to determine the subsurface geometry of the Mooki Fault. A nearly three-dimensional magnetic model, on the basis of the aeromagnetic data, will also be constructed to provide further insights to the subsurface structure of the fault.

6.2. Rock Properties

The source of the Mooki anomaly is still controversial. A plug-like correlative of the Warrigundi Intrusive in the south and a long dyke of hawaiite genetically related to the Tertiary Nandewar alkaline volcanic complex in the north were assumed by Ramsay and Stanley (1976) to produce the Mooki magnetic high. Later researchers showed that the

Warrigundi Intrusive bodies were part of the Early Permian Werrie Basalt rocks rather than Tertiary as shown on geological map of the region (Flood et al., 1988), and that the Currabubula Formation and Werrie Basalt with higher magnetic susceptibilities could be responsible for the anomalies over the Mooki Fault (Scheibner and Webster, 1982; Greentree and Flood, 1999; Schmidt, 1994)

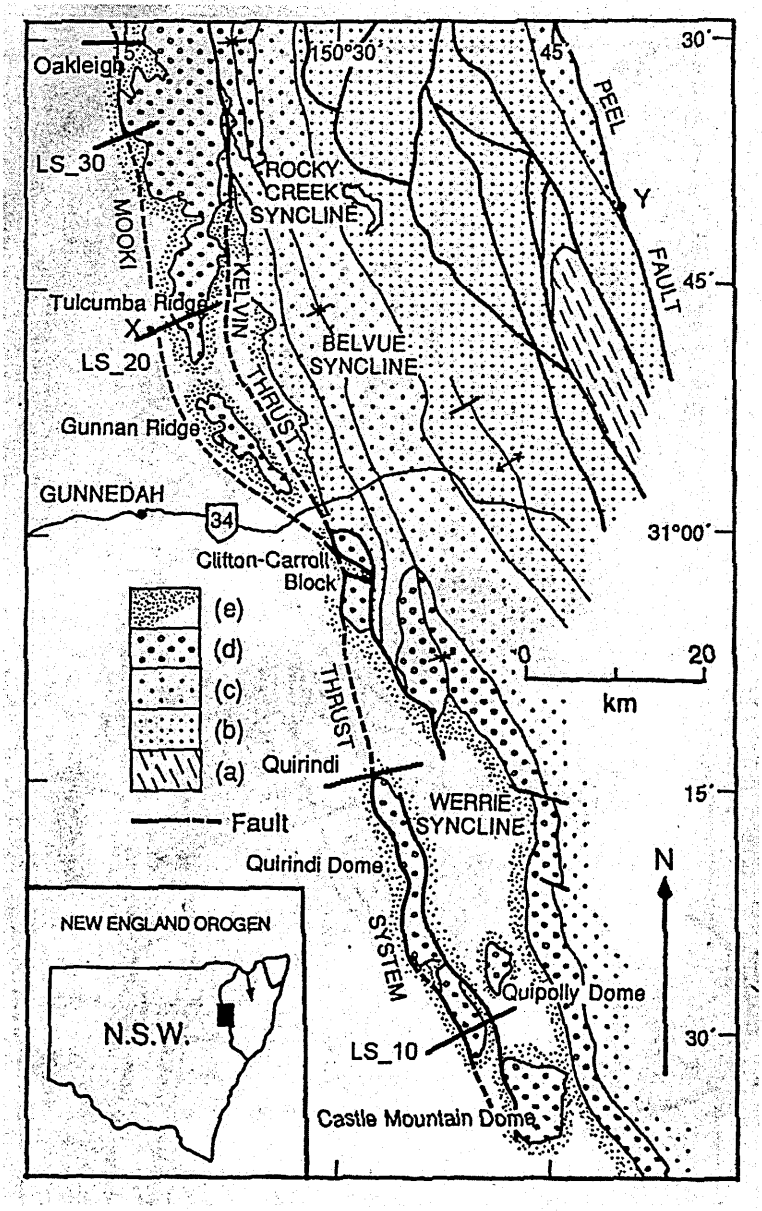

Figure 6.1a Location map of the Mooki Fault, the Werrie, Belvue and Rocky Creek Synclines (Modified after Liang 1991). Units represented (a) Early-Middle Devonian; (b) Late Devonian; (c) Early Carboniferous; (d) Late Carboniferous Currabubula Formation and equivalents; (e) Permian strata and recent alluvium. Lines indicate the position of the ground magnetic profiles and synthetic magnetic lines and show the profile name.

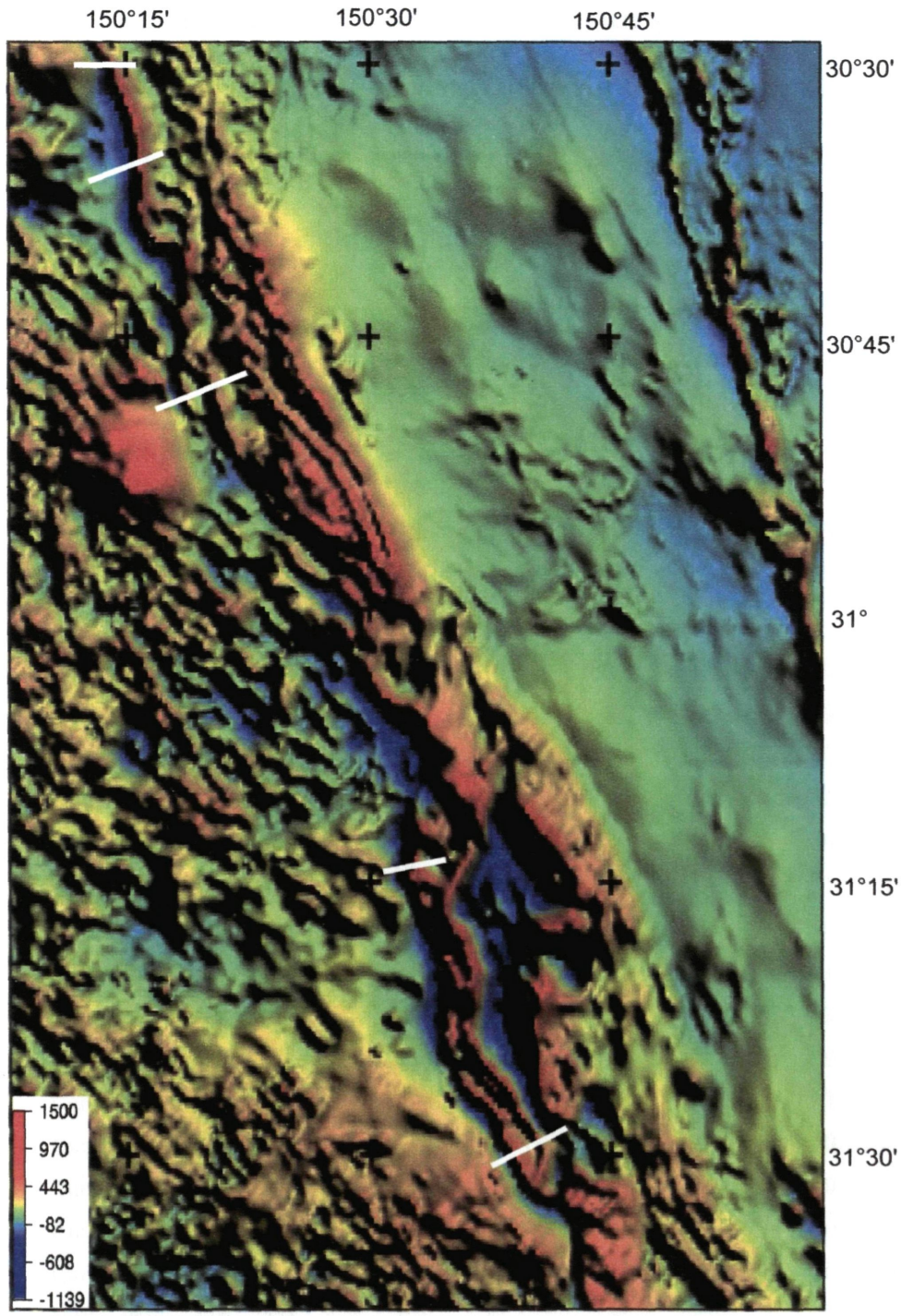

Figure 6.1b Location of the five magnetic traverses modelled in this chapter, shown on the colourdraped TMI magnetic image. From north to south, the magnetic traverses are named the Oakleigh, LS_30, LS_20, Breeza and LS_10 traverses.

Magnetic properties of the rocks along the Mooki Fault have been measured by various researchers on numerous rock samples from the Werrie Basalt, Merlewood/Currabubula

Formation units and undifferentiated Devonian-Permian sediments (Schmidt, 1994; Ramsay and Stanley, 1976). Compilations of these measurements are presented in Table 6.1. New measurements of the susceptibility of a conglomerate unit of the Currabubula Formation have been made in the field with a MS_2 susceptibility meter. The data is presented in Table 6.2.

Table 6.1 Susceptibility and NRM of samples from the Werrie Basalt and Currabubula /Merlewood Formation (Compiled from Schmidt, 1994)

Site	Rock Unit	NRM Dec (°)	NRM Inc (°)	NRM Int (μG)	κ (cgs) (10×10^{-6})	Q Ratio	Comments
	Werrie Basalt	25.7	70.1	1343	107	25.1	***
Werrie	Werrie Basalt	131.8	39.1	3136	2623	2.39	
Basin	Werrie Basalt	138.3	57.1	2162	562	7.69	
	Werrie Basalt	289.9	-56.9	1509	455	6.63	
	Average			2269	1213	5.57	
Limbs of the	Currabubula/Merlewood Fm.	348.9	-58.9	270	3205	0.17	
Werrie	Currabubula/Merlewood Fm.	336.9	-62.8	348.0	2872	0.24	
Syncline	Currabubula/Merlewood Fm.	340.8	-46.1	16.0	142	0.23	***
	Currabubula/Merlewood Fm.	235.1	-58.7	4228	3705	2.28	
	Currabubula/Merlewood Fm.	359.0	-54.2	263.1	1255	0.42	
	Currabubula/Merlewood Fm.	5.2	-75.0	86.5	120	1.44	***
	Currabubula/Merlewood Fm.	11.5	-61.3	218.0	532	0.82	***
	Currabubula/Merlewood Fm.	8.6	-64.6	93.1	139	1.34	***
	Currabubula/Merlewood Fm.	354.3	-49.8	646.6	3104	0.42	
	Currabubula/Merlewood Fm.	171.6	-42.8	460.1	2221	0.41	
	Currabubula/Merlewood Fm.	94.0	-77.1	2576	2323	2.22	
	Currabubula/Merlewood Fm.	148.3	-74.7	251.9	2766	0.18	
	Currabubula/Merlewood Fm.	16.2	-56.3	259.8	1607	0.32	
	Currabubula/Merlewood Fm.	2.5	21.8	3.61	19.2	0.38	***
	Currabubula/Merlewood Fm.	16.5	-67.8	169.5	1097	0.31	
	Currabubula/Merlewood Fm.	150.3	32.4	2686	1593	3.37	
	Average			1080.8	2340	0.74	

Note: the samples with *** were excluded for calculation of the average susceptibility and Q value due to weathering or lightning on the samples. Explanation of Table 6.1 headings: Site, for sampled location, NRM, for measured natural remanent magnetization, κ, for susceptibility, Q for Koenigsberger ratio.

Table 6.2. The Susceptibility of the Conglomerates from Currabubula Formation near Werris Creek.

Location		Average κ (10×10^{-6} cgs)		Number of readings	
Easting	Northing	Matrix	Pebble	Matrix	Pebble
270997	6528375	2090	1105	11	11
271275	6528353	2118	1009	6	4

Note: The measurement of the susceptibility was conducted on the weathered conglomerate rocks. The data is only for reference. Explanation of Table 6.2 headings: Easting and Northing for Australian Map Grid 56 location of the susceptibility reading point. κ for susceptibility.

6.3 Modelling of the ground magnetic transverses over the Mooki Fault.

The magnetic data collected across the Mooki Fault was modelled using Modelvision Pro 5.0 ^{TM} – an interactive potential field modelling package supplied by Encom Technology. Local geomagnetic parameters for each traverse are shown in Table 6.3.

In order to eliminate anomalies due to anthropogenic artificial materials and to reduce topographic effects on the magnetic anomaly, an upward continuation filter of 30 m was applied to all ground magnetic data before the data was modelled. The anomalies were initially modelled by forward calculation using magnetized polygons. Once a reasonable model was achieved then inversion was used to produce a best-fit model for the observed anomalies.

Table 6.3 Local geomagnetic parameters

Parameters Transverses	Magnetic field intensity (nT)	Magnetic field Dec (°)	Magnetic field Inc (°)	Line Length (km)	Line Mean direction (True) (°)
Oakleigh	55621	11.3	-61.2	8.9	91
Quirindi	56130	11.7	-62.1	7.9	72
LS_30	55690	11.2	-61.3	30	70
LS_20	55784	11.3	-61.5	30	70
LS_10	56165	11.6	-62.2	17	70

Line Oakleigh

Line Oakleigh was surveyed to the north of the Tulcumba Ridge (Figure 6.1). The data are plotted in Figure 6.2 and the major peak has an amplitude of 3800 nT. The surveyed area is covered by alluvium and therefore no outcrops can be linked to this magnetic anomaly.

Line Oakleigh was constrained by previous geophysical surveys undertaken in the vicinity, consisting of both seismic data (Korsch et al., 1993a, b, 1997) and magnetic data (Ramsay and Stanley, 1976), and could provide the basic interpretation to be used on the other lines. The anomaly was assumed by Ramsay and Stanley (1976) to be produced by a 20± km long dyke of hawaiite emplaced along the Mooki Fault, with an eastward dip of 25°. Interpretation of the seismic data (Korsch et al., 1993a, 1997) also inferred that the fault dipped to the east with an angle of 25°. In consideration of constraints from both the seismic data and magnetic data, a dyke-like body with an eastward dip of 25° was initially used to model the observed anomalies at Oakleigh over the Mooki Fault (Figure 6.2a). The best-fit model from inversion shows that a very high susceptibility of 15500 × 10^{-6} cgs for the modelled body is required to fit the observed anomaly. Two small bodies with susceptibilities of 6000 and 4500× 10^{-6} cgs, respectively, were introduced to more closely match the observed high-frequency anomalies (Figure 6.2b). However, no available evidence supports such a high susceptibility unit and this model is not possible.

Alternatively, the magnetic anomalies over the Mooki Fault may be due to the contrast between higher magnetic susceptibilities of the Currabubula Formation and/or Werrie Basalt and the Late Permian and Triassic sediments (Sydney-Gunnedah basin) to the west (Scheibner & Webster, 1982; Greentree and Flood 1999; Schmidt, 1995). Therefore, the magnetic source is assumed to be a magnetic unit in the Late Carboniferous Currabubula Formation. The observed anomalies were modelled as overturned bedding as suggested by Carey (1934a) for the region west of Werrie Creek and later Liang (1989, 1991) for the area west of Keepit Dam

on Tulcumba Ridge (Figure 6.2c). The modelled tabular body with a dip of 66° to the east is consistent with the geological observations in the Tulcumba Ridge, where the overturned ignimbrite units dip at this angle (Liang, 1989, 1991). Liang (1991) suggested that the structure in the Tulcumba Ridge shows a syncline-anticline pair with the western limb of the anticline becoming overturned, and is a thrust propagation structure (Figure 2.4). Liang (1991) also noted that the youngest of the overturned rocks could be Early Permian Lavas (i.e. part of the Werrie Basalt).

The average value of the measured susceptibility from the Late Carboniferous Currabubula Formation near Werris Creek in the south is 2340×10^{-6} cgs (Table 6.1). No susceptibility measurements were taken along line Oakleigh due to alluvium cover. The susceptibility of 2340×10^{-6} cgs, therefore, was initially used to model the observed data, but is too low to explain the peak. An increase in the susceptibility to 6000×10^{-6} cgs brings a match to the amplitude of the anomaly (Figure 6.2c). The major body has an azimuth of 332° and a depth extension of 2.5 km. The tabular bodies within the major body are used to get the best fit, probably indicating the heterogeneous magnetic sources within the overturned beddings. (Figure 6.2c).

Because geological structure in areas of no outcrop is inferred, where the magnetic survey was conducted, the overturned anticline structure could not be excluded and was also used as the base to model the observed magnetic anomalies. Figure 6.2d shows the simplified overturned anticline structure with two tabular bodies. The modelling indicates that the east limb required an extremely high susceptibility double the value of the susceptibility used in the western limb. This is unlikely to occur for the same bed. As well, to get the observed anomaly to fit, the eastern limb is narrower than the overturned western limb. The modelling results thus suggest that the overturned anticline model does not explain the observed magnetic anomalies.

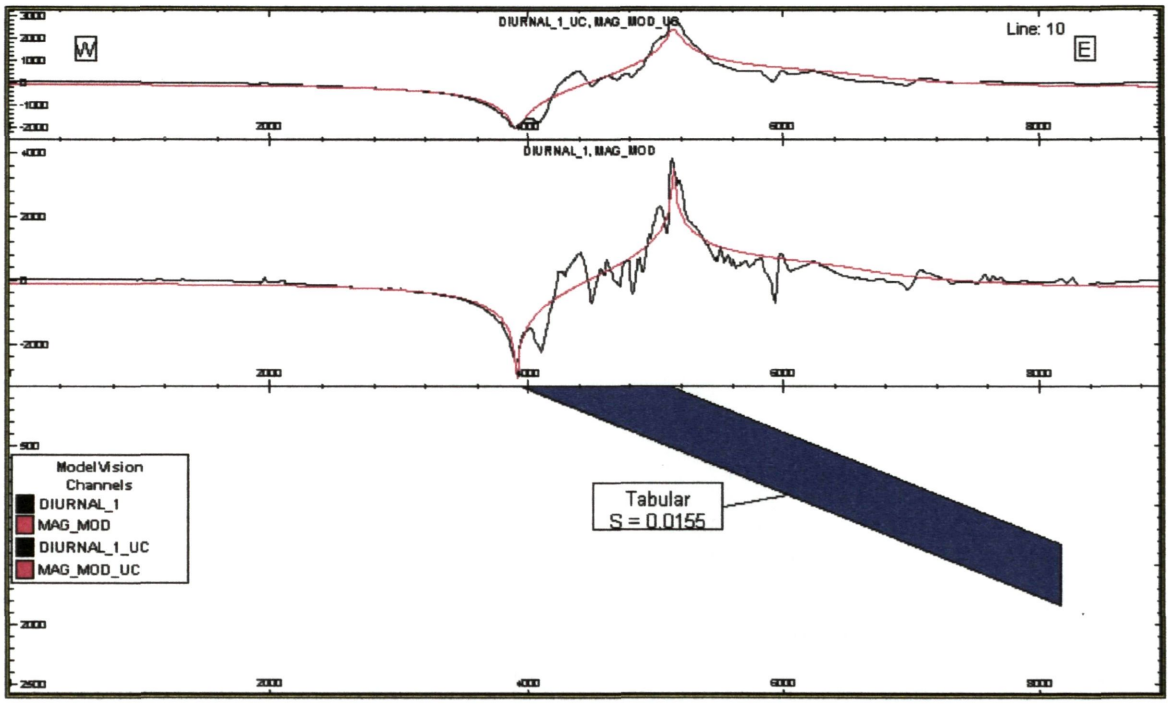

Figure 6.2a. 2-D magnetic model along the Oakleigh traverse, north of Gunnedah (cross-section view). The observed data was modelled with the parameters used by Ramsay and Stanley (1976). The tabular body dips to the east at 25° with an azimuth of 340°, V/H=1. See Figure 6.1 for location of the cross-section.

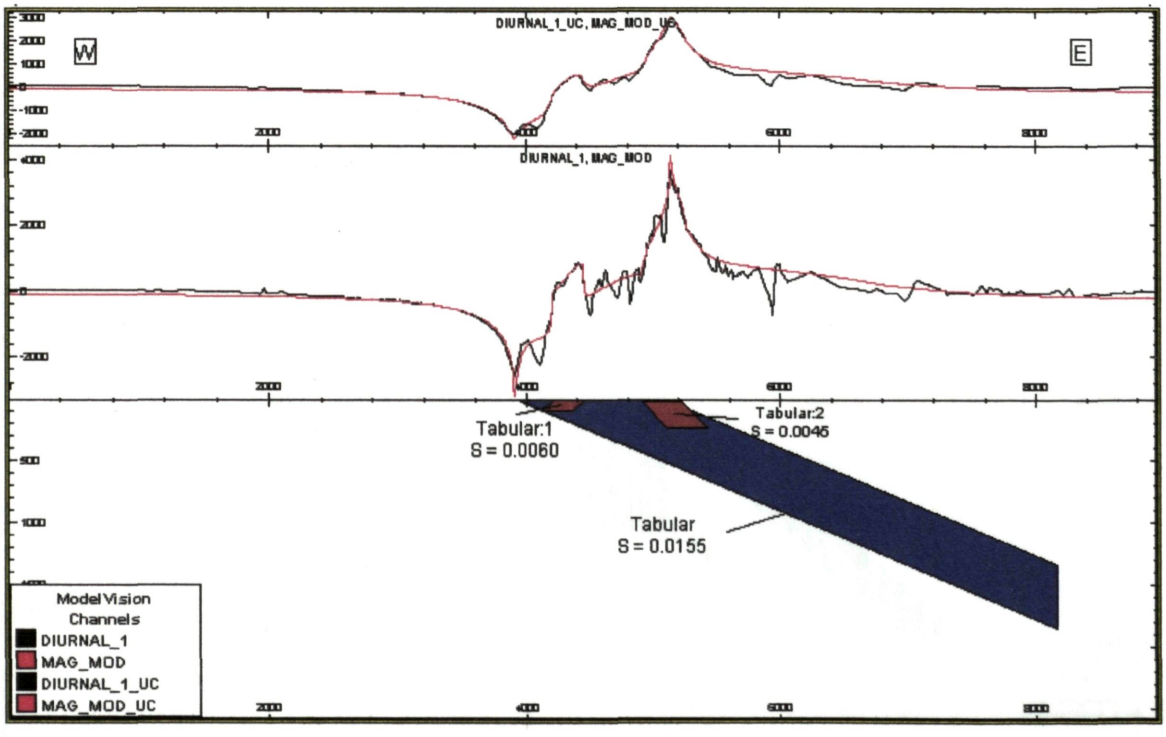

Figure 6.2b. 2-D magnetic model along the Oakleigh traverse, north of Gunnedah (cross-section view). The observed data was modelled with the parameters used by Ramsay and Stanley (1976). The tabular body dips to the east at 25° with an azimuth of 340°, two small bodies were introduced to match the observed high-frequency anomalies V/H=1. See Figure 6.1 for location of the cross-section.

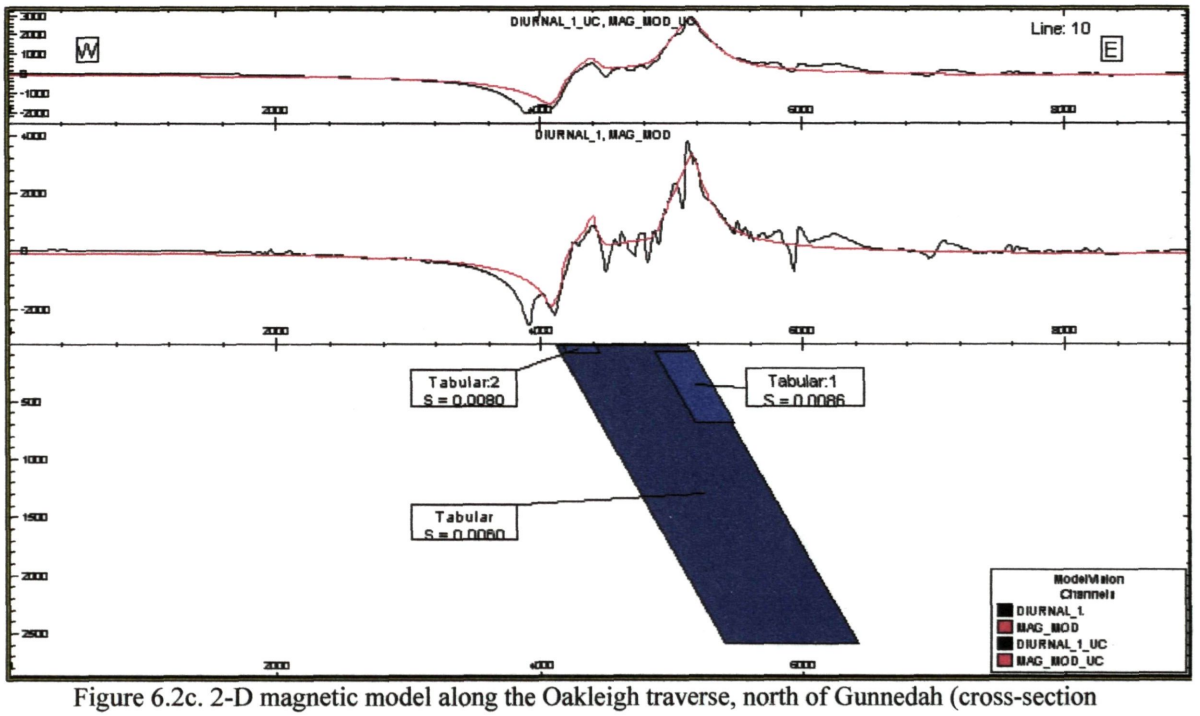

Figure 6.2c. 2-D magnetic model along the Oakleigh traverse, north of Gunnedah (cross-section view). The observed data was modelled as overturned bedding. The main tabular body dips to the east at 66° with an azimuth of 332°, two small bodies were introduced to match the observed high-frequency anomalies V/H=1. See Figure 6.1 for location of the cross-section.

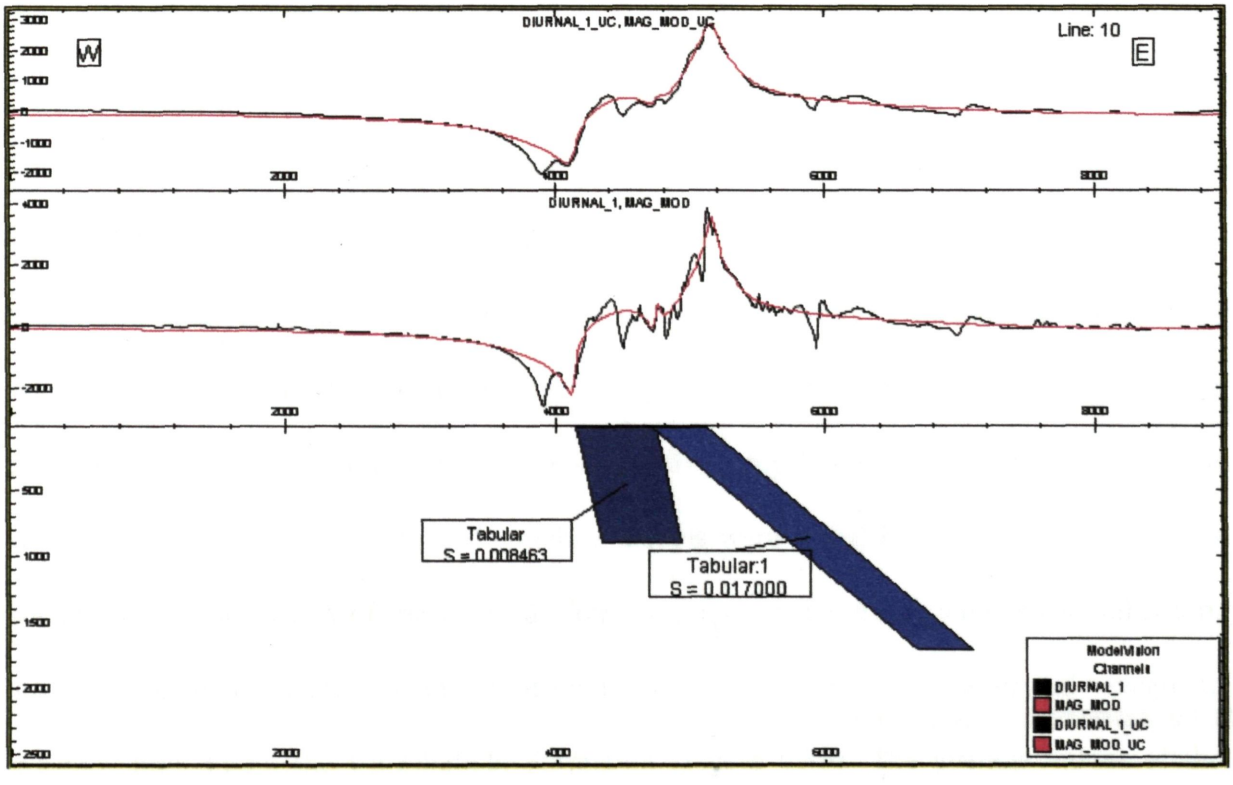

Figure 6.2d. 2-D magnetic model along the Oakleigh traverse, north of Gunnedah (cross-section view). The observed data was modelled as an overturned anticline, V/H=1. See Figure 4.8 for location of the cross-section.

Line Breeza, Quirindi

Line Breeza was surveyed in January 2004 to the east of the Breeza village. The data is plotted in Figure 6.3 and the major peak has an amplitude of around 4000 nT. The surveyed area is covered by alluvium and no outcrops are related to the observed anomaly.

The anomaly was attributed to a pluglike correlative of the Warrigundi Igneous Complex (Ramsay and Stanley, 1976). This assumption is questioned because the recent research by Flood et al (1988) indicated that the Warrigundi Igneous Complex is Early Permian instead of Tertiary. Although the magnetic source as proposed by Ramsay and Stanley is not likely to be Tertiary, a sheet-like body emplaced along the Mooki Fault was initially used to model the observed anomaly. The tabular body dipping to the east at an angle of 25° matched the observed data over the Mooki Fault. The inversion results indicated that the susceptibility of the modelled tabular body is very high, and a value of 12800×10^{-6} cgs was required to match the observed data (Figure 6.3a).

Alternatively, the magnetic source is assumed to be a magnetic unit in the Late Carboniferous Currabubula Formation or Early Permian Werrie Basalt on the basis of the interpretation of the aeromagnetic data and rock property measurements. A conglomerate unit of the Currabubula Formation outcrops 2 km south of the surveyed line, and rock properties were determined from it for magnetic modelling. The geometry of the magnetic source was modelled using the anticlinal structure observed by Carey (1934a) and Liang (1991). Both overturned bedding and overturned anticline models were tested because the survey line is located in the north end of the Quirindi dome and the survey area is covered by alluvium. Initially the main magnetic anomaly at Quirindi was modelled with the strongly magnetic western limb being the Currabubula Formation (Figure 6.3b). The average values of the susceptibility from the nearest conglomerate unit of the Currabubula Formation 2 km south of the magnetic line are 2100×10^{-6} cgs (this study) and 2340×10^{-6} cgs (Schmidt, 1994), and

the Werrie Basalt has a susceptibility of 2300 × 10^{-6} cgs, all values being too low to produce the observed amplitude of the anomaly. A doubling of the susceptibility to 5400 × 10^{-6} cgs brings a good match to the amplitude of the anomaly. The best fit modelling indicates that the tabular body has a dip of 52° to the east with an azimuth of 339°, and a width of 1.8 km. the modelled structure could be interpreted as an overturned magnetic unit of the Late Carboniferous Currabubula Formation or the Early Permian Werrie Basalts. The width of the modelled body supports an observation by Russell (1981) on the width of 2 km for the Late Carboniferous Currabubula Formation. Again a small tabular body was introduced to match the high frequency feature to get the best fit.

Furthermore, in modelling the overturned anticline documented by Liang (1991), the structure was simplified with two main tabular bodies to model the observed anomaly. Figure 6.3c shows the simplified overturned anticline structure composed of the two tabular bodies. Both main bodies have a width of 750 m, and a susceptibility of 4500 × 10^{-6} cgs. The modelling results indicate that both the overturned anticline and overturned bedding models could be used to model the observed magnetic anomalies.

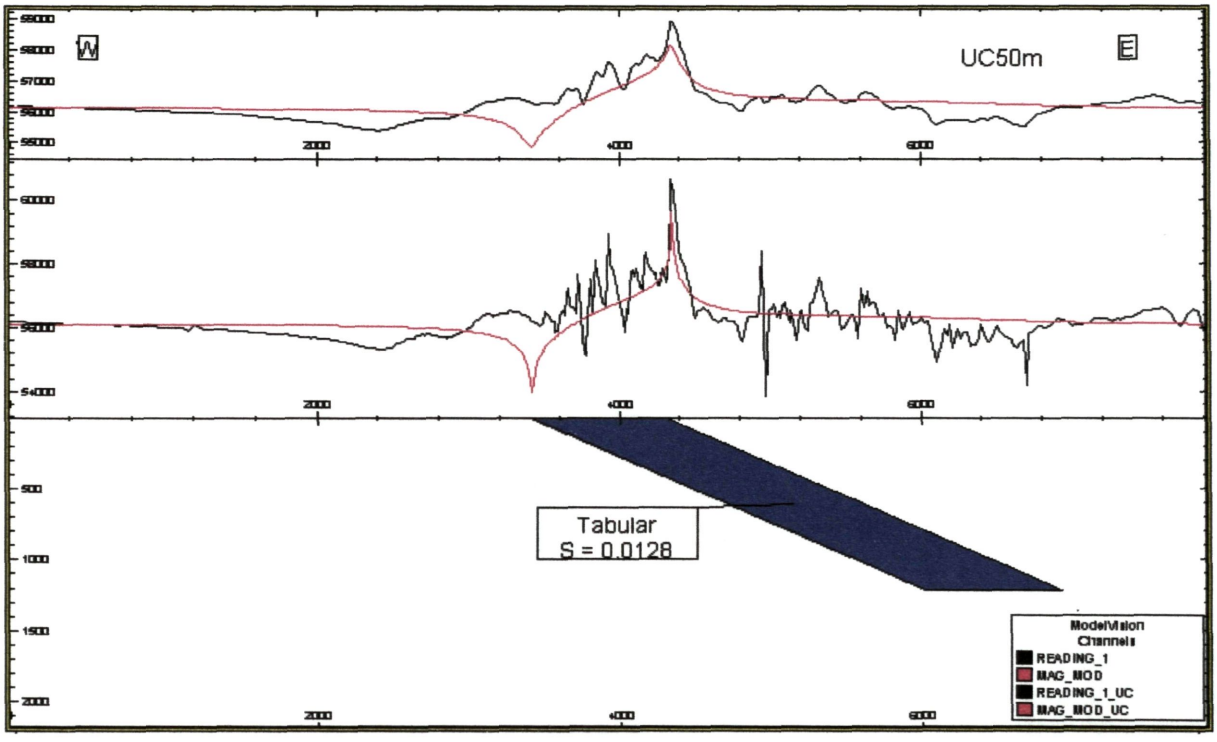

Figure 6.3a. 2-D magnetic model along the Breeza traverse, east of Breeza (cross-section view). The observed data was modelled with the parameters used by Ramsay and Stanley (1976). The tabular body dips to the east at 25° with an azimuth of 340°, V/H=1. See Figure 6.1 for location of the cross-section.

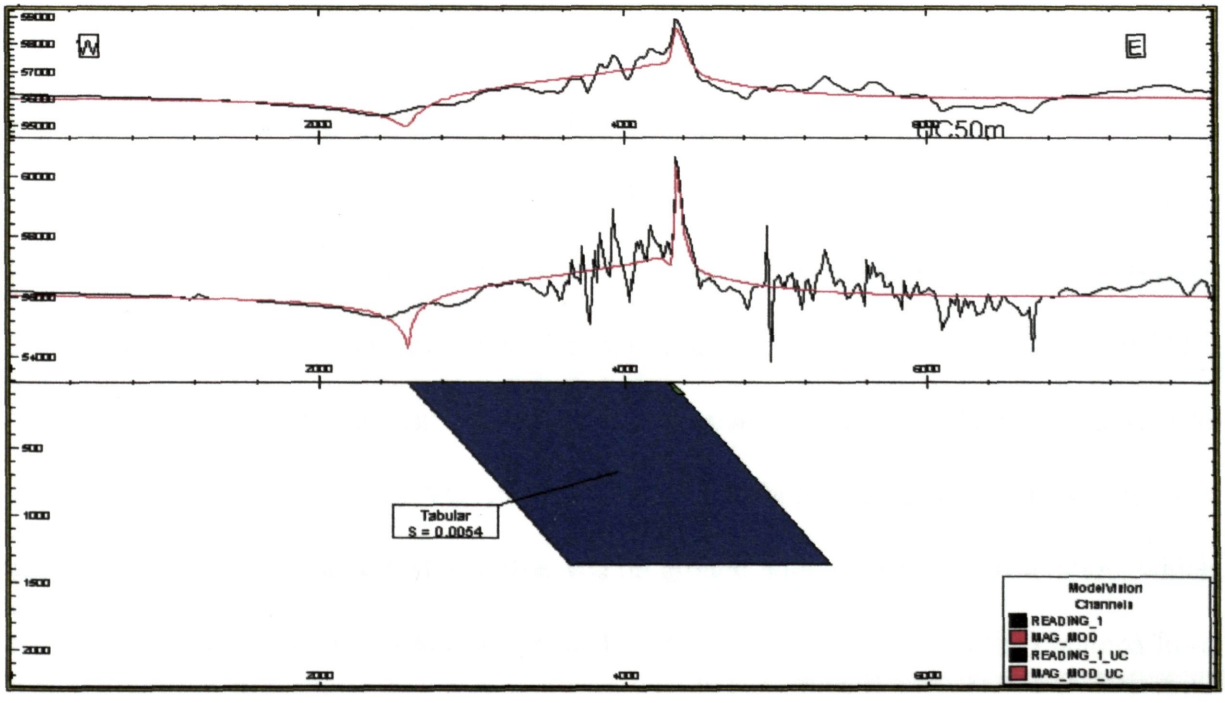

Figure 6.3b. 2-D magnetic model along the Breeza traverse, east of Breeza (cross-section view). The observed data was modelled as overturned bedding as proposed by Liang (1991). The main tabular body dips to the east at 52° with an azimuth of 339°, a small body was introduced to match the observed near surface feature, V/H=1. See Figure 6.1 for location of the cross-section.

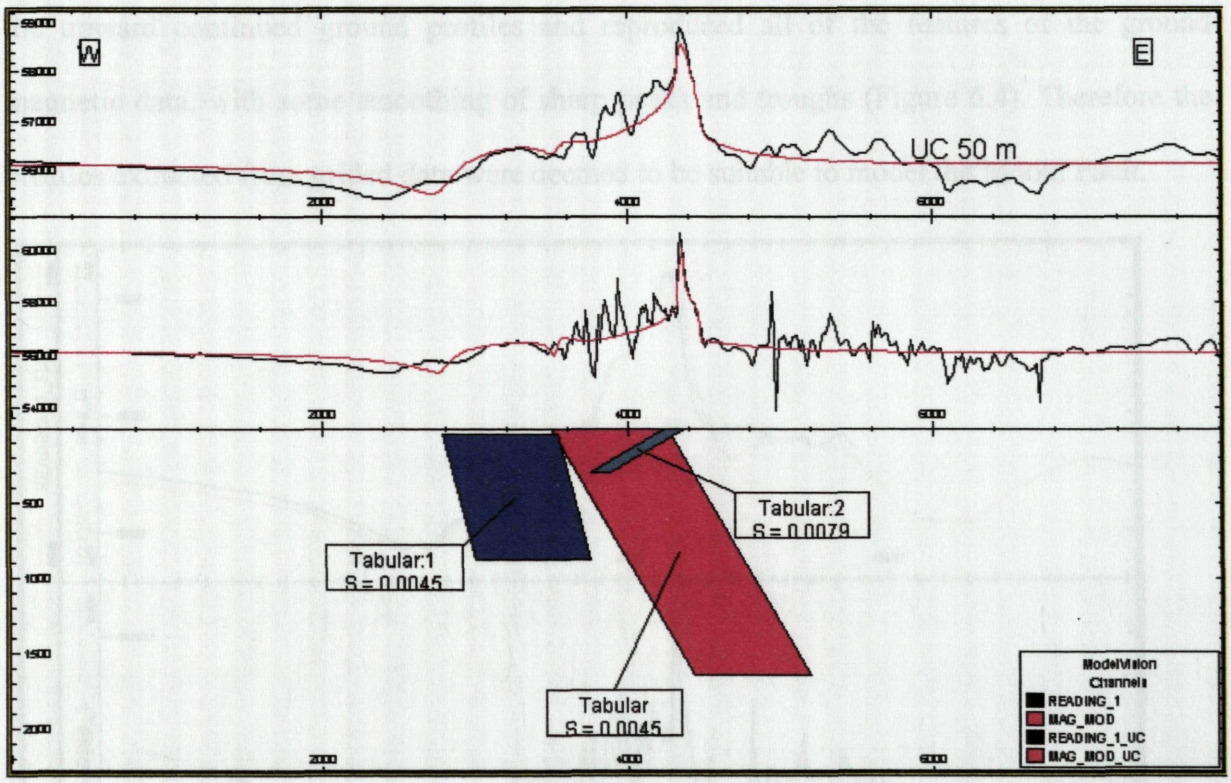

Figure 6.3c. 2-D magnetic model along the Breeza traverse, east of Breeza (cross-section view). The observed data was modelled as an overturned anticline. A small body was introduced to match the observed near surface feature, V/H=1. See Figure 6.1 for location of the cross-section.

6.4 Modelling of the lines extracted from the aeromagnetic data

In order to get better understanding of the subsurface geometry of the Mooki Fault, three lines were sampled from the aeromagnetic dataset and were modelled to get a constraint for the Mooki Fault on a regional scale. The aeromagnetic dataset used is the Discover 2000 Narrabri dataset, Peel dataset and Liverpool Plain aeromagnetic dataset, which were described in Chapter three. A simple test was made to determine whether the synthetic magnetic lines have expressed all magnetic features observed on ground with a reasonable resolution, which could be used to model the subsurface geometry of the Mooki Fault. A profile obtained from the grided aeromagnetic data was compared with the corresponding magnetic profile conducted on the ground, which was upward-continued to a level at which the aeromagnetic data was collected. The profiles from the grided aeromagnetic data compared favourably with

the upward continued ground profiles and reproduced all of the features of the ground magnetic data, with some smoothing of sharp peaks and troughs (Figure 6.4). Therefore the profiles extracted from grided data were deemed to be suitable to model the Mooki Fault.

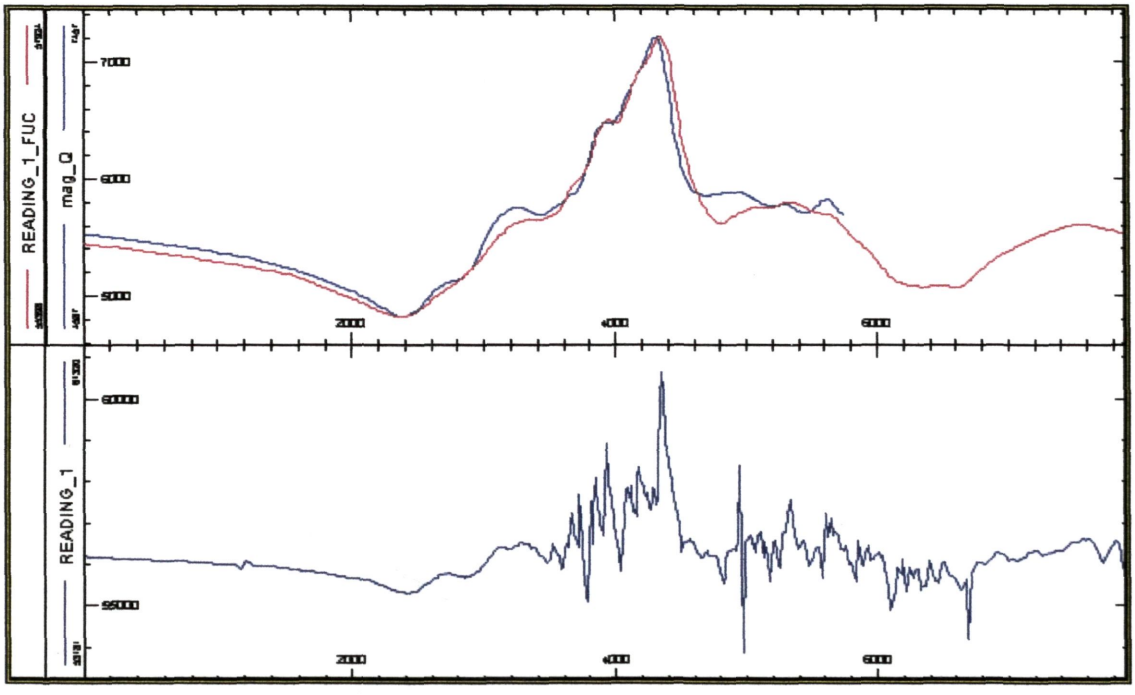

Figure 6.4. Comparison of the extracted profiles from the gridded aeromagnetic data with the upward continued ground magnetic profiles. All the main features of the ground magnetic data were reproduced from the gridded aeromagnetic data.

Line LS_10

The line LS_10 is located at the southern part of the Quirindi Dome (Figure 6.1). Along Line LS_10 the Late Carboniferous Currabubula Formation composed of polymictic conglomerate and sandstone outcrops to the east of the Mooki Fault and Quaternary sediments to the west (Offenberg, 1967). The magnetic traverse is extracted from the Liverpool Plains dataset surveyed by Geoscience Australia (former AGSO) in 1995. The height of acquisition of survey data above the ground surface is 80m. The line is plotted in Figure 6.5, and has three major peaks.

The high amplitude peak between 8000 and 9000 m corresponding to the Mooki Fault, was first modelled with a single tabular body to test the subsurface structure of the Mooki

Fault as proposed by Ramsay and Stanley (1976). The tabular body has a dip of 25° to the east, as used by Ramsay and Stanley (1976), and an azimuth of 335°. The anomaly was assumed to be produced by a correlative of the Warrigundi Igneous Complex (Ramsay and Stanley, 1976). The susceptibility of 1000× 10^{-6} cgs proposed by Ramsay and Staley (1976) was used to model the observed data but could not produce a match of the first major peak. An extremely high susceptibility of 9700 × 10-6 cgs is required to achieve this (Figure 6.5a).

It is obvious that the single tabular body could not produce a match for the anomalies related to the Quirindi Dome. Relatively complex models were developed to match the observed data. Based on the geological map (Brown et al., 1992), the first two peaks correspond to the Quirindi Dome. Therefore an overturned anticline model was developed to fit the first two peaks (Figure 6.5b, c). Figure 6.5b indicates a case in which the top of the anticline was removed, the two beds represent the west and east limbs of the overturned anticline. The perspective map is shown in Figure 6.5c. Modelling starts with two east-dipping tabular bodies corresponding to the two observed peaks, once a preliminary match was reached, then inversion was used to get a best fit to the observed data. The best-fit modelling result indicates that the western limb has an eastward dip of 36° and an azimuth of 333°. The east limb has an eastward dip of 18° and an azimuth of 340°. The measured average susceptibility of 2100 × 10^{-6} cgs (Table 6.2) and 2340 × 10^{-6} cgs (Table 6.1) by Schmidt (1994) for the Late Currabubula Formation was not enough to produce the observed amplitude. An increased susceptibility of around 5000 × 10^{-6} cgs was used to match the observed data.

The best match of the magnetic anomalies associated with the Quirindi Dome is produced by an overturned anticline structural model (Figure 6.5d, e), which was proposed by Carey (1934a) for the west of the Werrie Syncline and later developed by Liang (1991) at the Tulcumba Ridge. On the basis of the previous model, a susceptibility of 5000 × 10^{-6} cgs was used to get a fit to the observed anomalies. The perspective map shows a 3 dimensional

overturned anticline (Figure 6.5e). The axis of the anticline has an azimuth of 340°, which is consistent with the geological observations by Carey (1934).

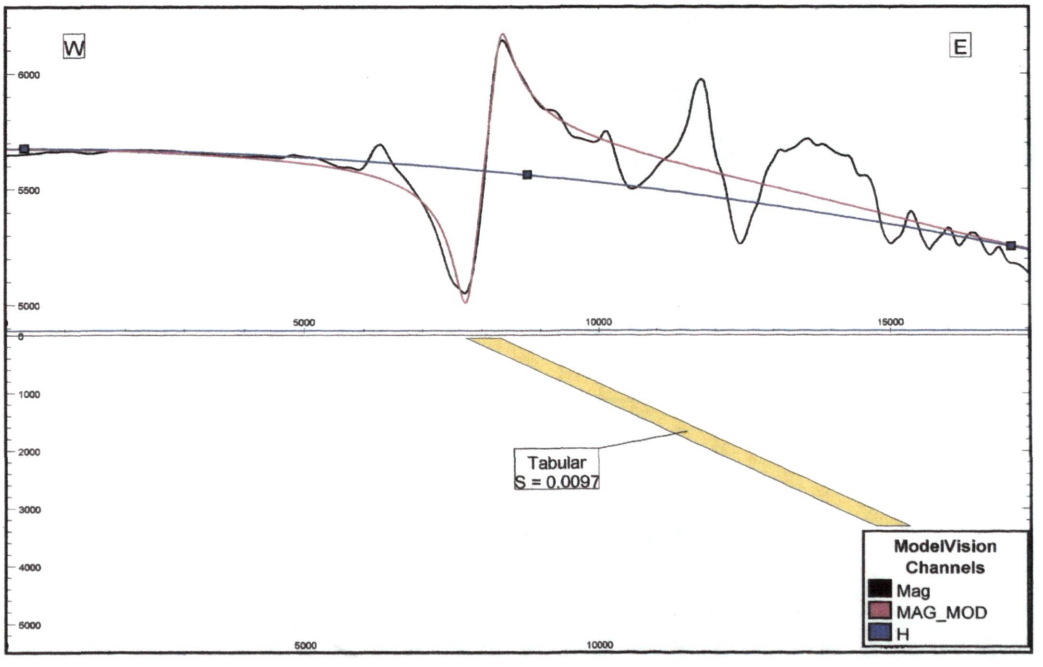

Figure 6.5a. 2-D magnetic model along Line LS_10 across the Quirindi Dome (cross-section view). The data was modelled with the parameters used by Ramsay and Stanley (1976). The tabular body dips to the east at 25° with an azimuth of 340°, V/H=1. See Figure 6.1 for location of the cross-section.

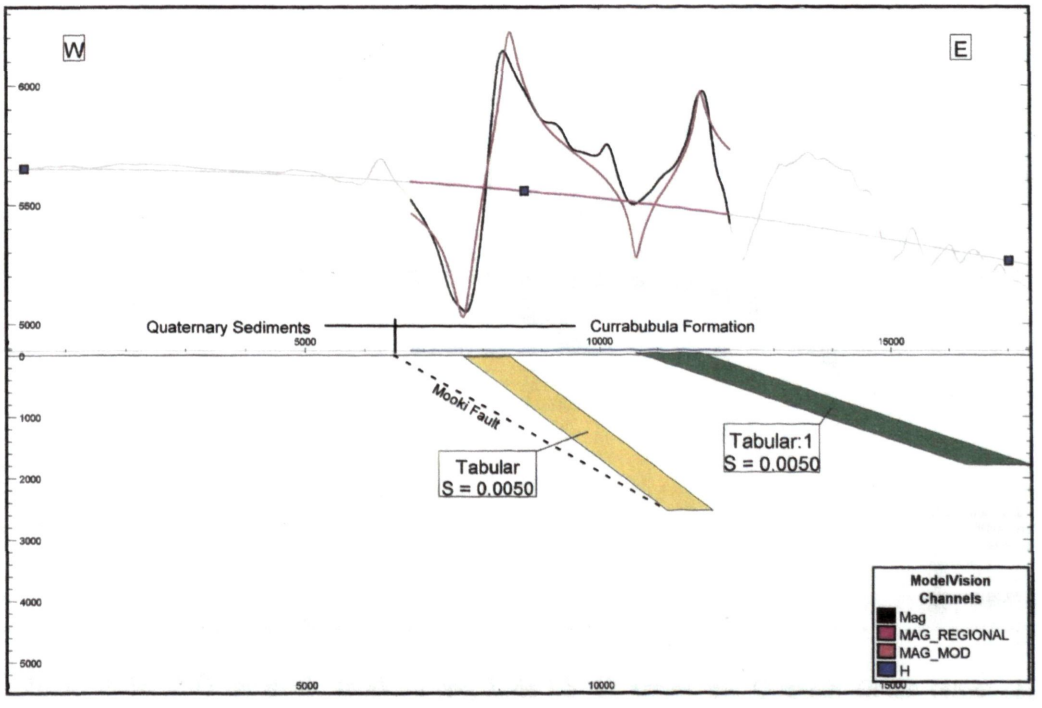

Figure 6.5b. 2-D magnetic model along Line LS_10 across the Quirindi Dome (cross-section view). The data was modelled as two limbs of an overturned anticline, V/H=1. See Figure 6.1 for location of the cross-section.

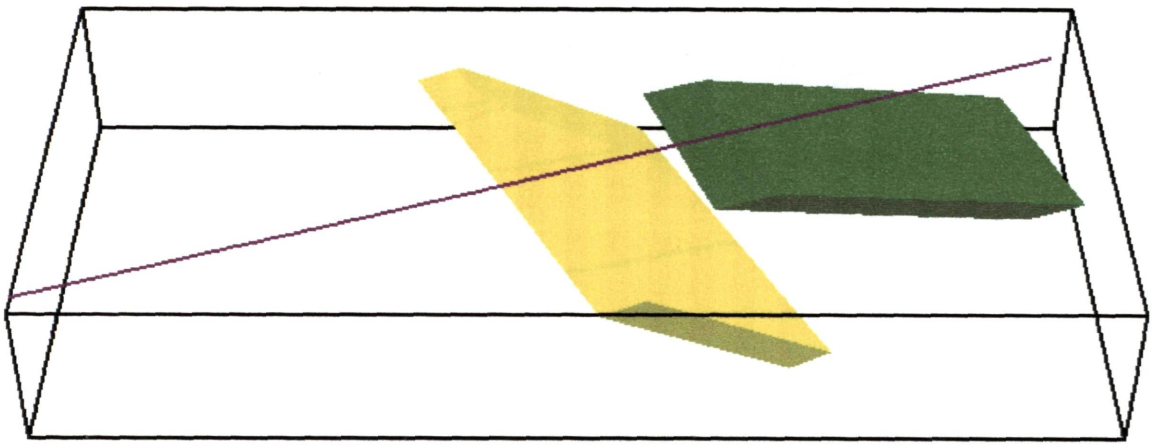

Figure 6.5c Perspective view of Figure 6.5b.

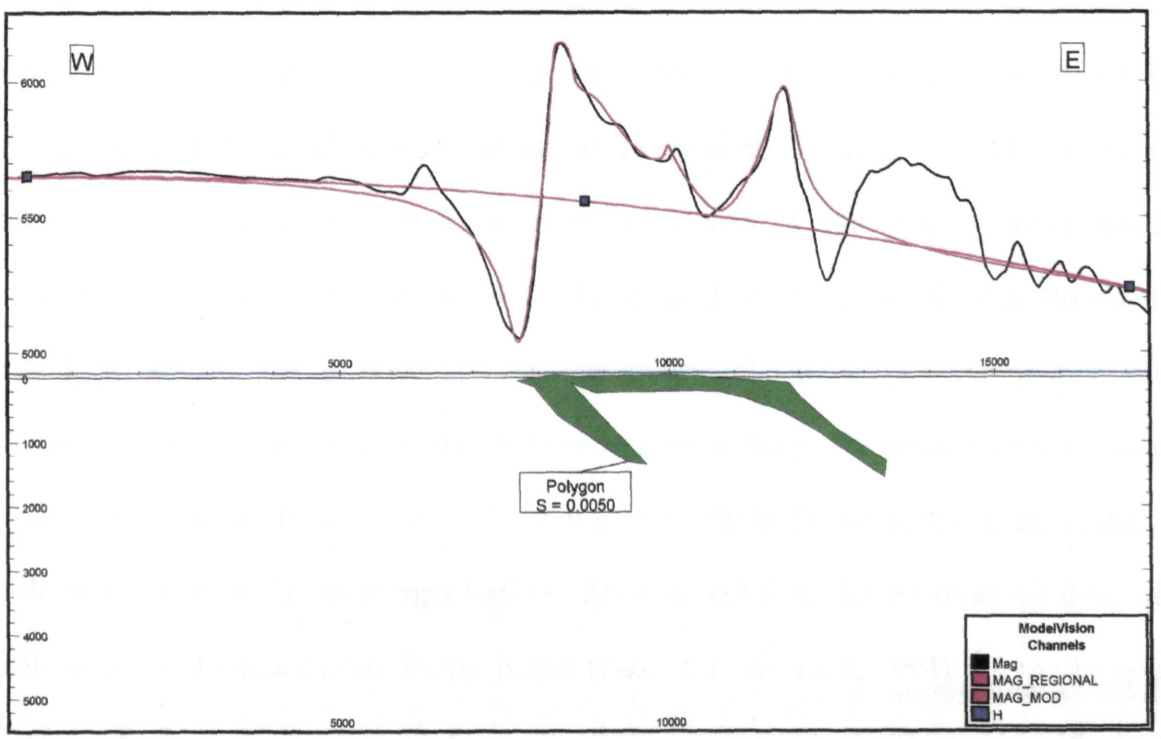

Figure 6.5d. 2-D magnetic model along Line LS_10 across the Quirindi Dome (cross-section view). The data was modelled as an overturned anticline, V/H=1. See Figure 6.1 for location of the cross-section.

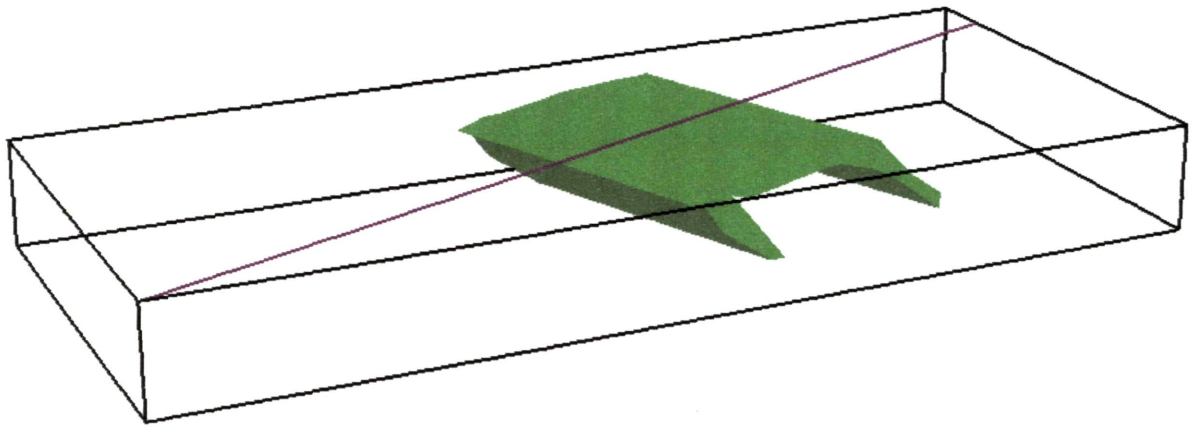

Figure 6.5e. Perspective view of Figure 6.5c.

Line Ls_20

The Line Ls_20 is located at the southern part of the Tulcumba Ridge (Figure 6.1), and is plotted in Figure 6.6. The two peaks seen between 4000 – 9000 m are associated with the Tulcumba Ridge, and are inferred to be produced by the Currabubula Formation, based on the interpretation of aeromagnetic data. A susceptibility of 3000×10^{-6} cgs was used for the polygon bodies to match the observed magnetic anomalies. The line is initially explained by two eastward dipping polygon bodies with an azimuth of 340° (Figure 6.6a), which is consistent with general trend of the Mooki Fault based on the geological map (Brown et al., 1992). A best fit was produced by an introduction of a remanence contribution with a declination of 126° and inclination of 53° for the western body. The remanence of the western body is approximately consistent with that of the Werrie Basalt to the south (Table 6.1, Schimidt, 1994). A Koenigsberger Ratio of 2.9 was used to model the observed data, which falls into the Q range of the Werrie Basalt (Table 6.1, Schimidt, 1994). As can be seen in Figure 6.6b the resulting calculated anomaly shows a better fit to the observed profile than the previous model (Figure 6.6a). This model probably represents an overturned anticline with the removal of the top part.

Alternatively a good fit could be produced by a similar structural model, with a different azimuth and susceptibility, without remanence contribution (Figure 6.6c). In this model, both tabular bodies have an azimuth of around 280° and the susceptibility of the 5000 × 10^{-6} cgs. The azimuth of around 280° is not supported by the NNW trending of the Mooki Fault on the basis of the geological map of Brown (1992).

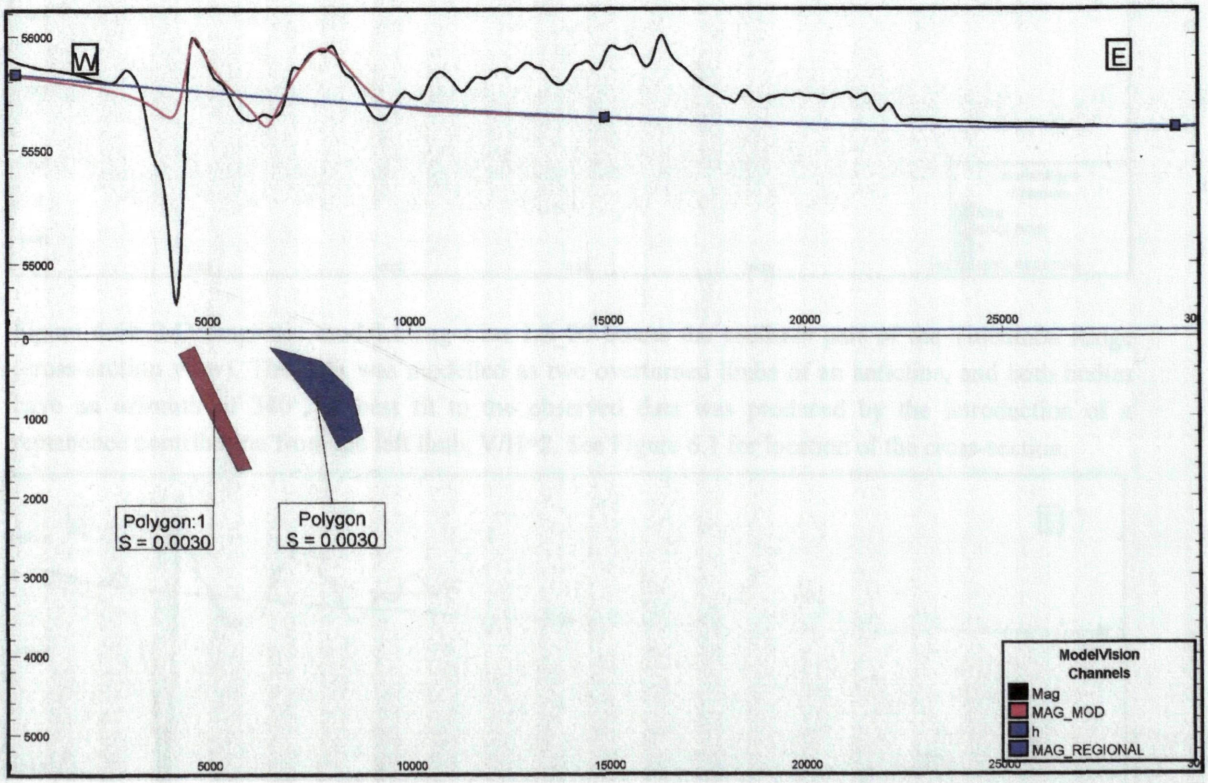

Figure 6.6a. 2-D magnetic model along Line LS_20 across the southern part of the Tulcumba Ridge (cross-section view). The data was modelled as two overturned limb of an anticline, and both bodies have an azimuth of 340°. The calculated profile could not fit the observed data, V/H=2. See Figure 6.1 for location of the cross-section.

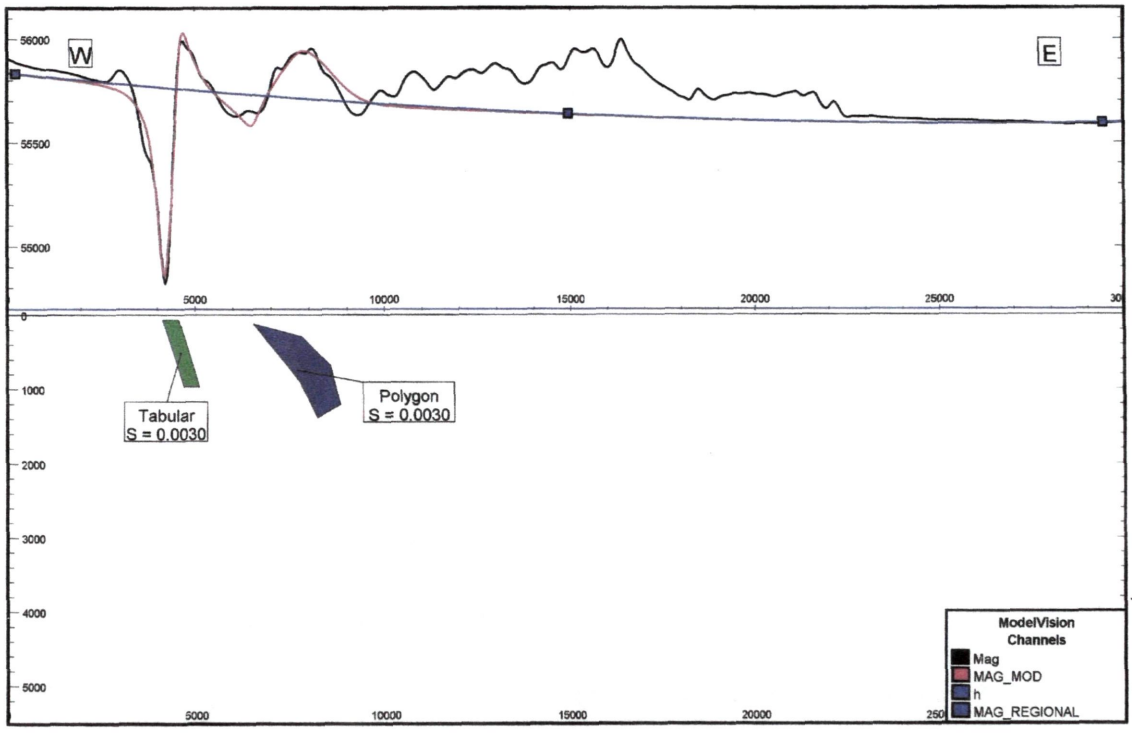

Figure 6.6b 2-D magnetic model along Line LS_20 across the southern part of the Tulcumba Ridge (cross-section view). The data was modelled as two overturned limbs of an anticline, and both bodies have an azimuth of 340°. A best fit to the observed data was produced by the introduction of a remanence contribution from the left limb, V/H=2. See Figure 6.1 for location of the cross-section.

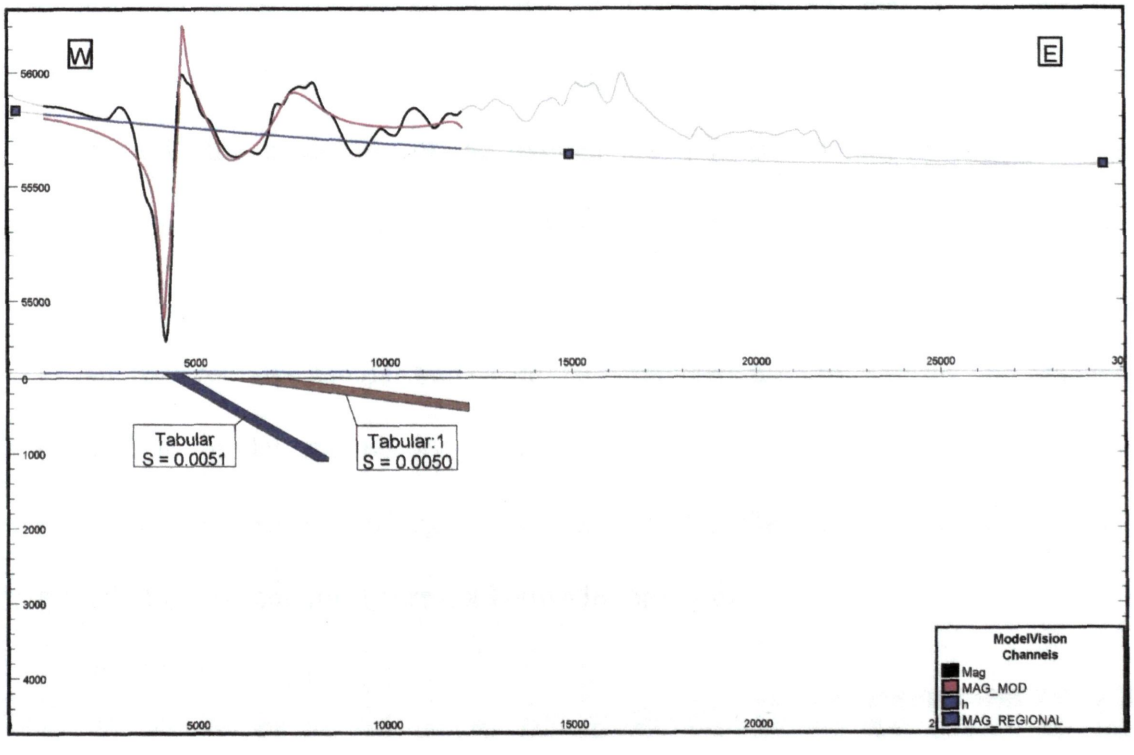

Figure 6.6c. 2-D magnetic model along Line LS_20 across the southern part of the Tulcumba Ridge (cross-section view). The data was modelled as two overturned limbs of an anticline, and both bodies have an azimuth of 280°, which is not supported by geology (Brown et al, 1992), V/H=2. See Figure 6.1 for location of the cross-section.

Line LS_30

The line LS_30 is located to the north of the Tulcumba Ridge (Figure 6.1). Along the line the Late Carboniferous Currabubula Formation outcrops to the east of the Mooki Fault and the Late Early Permian Maules Creek Formation composed of carbonaceous claystone, sandstone and siltstone outcrops to the west (Brown et al, 1992). The data is plotted in Figure 6.7 and is best explained by a tabular body, which has an eastward dip of 56°, and azimuth of 335° (Figure 6.7a). The anomaly was assumed to be produced by the Late Carboniferous Currabubula Formation and therefore, initially, the average measured susceptibility of the Currabubula Formation near Quirindi was used to model the observed data. However, the measured susceptibility of the Currabubula Formation could not produce a best match for the observed anomaly, and a minimum susceptibility of 8000×10^{-6} cgs is required to fit the data. This "representive" susceptibility probably indicates a remanence contribution which is similar to the present geomagnetic field. Schmidt (1994) (Table6.1) has measured such remanences for units of the Currabubula Formation. No attempt was made to use a specific remanence in the modelling of the anomaly. The modelled best-fit subsurface structure possibly represents the western limb of the overturned anticline, as suggested by Liang (1991).

Alternatively, the tabular body with the parameters used by Ramsay and Stanley (1976) was used to model the observed data (Figure 6.7b). In this case, an extremely high susceptibility of 16800×10^{-6} cgs is required to fit the observed amplitude. Rocks with such extremely high susceptibility are not known in the region.

6.5. Discussions of the modelling results

This study models two ground magnetic transverses and three synthetic magnetic lines extracted from the aeromagnetic data, which extend over a strike length of 120 km from Quirindi in the south to Oakleigh near Maules Creek in the north. Most of the magnetic profiles could be modelled with simple tabular magnetic bodies. All profiles could be modelled with the geometry proposed by Ramsay and Stanley (1976), but extremely high susceptibilities were required to match magnetic anomalies, suggesting that the model developed by them might not be a geological realistic explanation of the anomaly.

The best fit modelling of the five magnetic profiles produced three different geological structural models. In the Manilla map sheet, both the ground magnetic line Oakleigh and the extracted magnetic line LS_30 were best explained by a single tabular body with an eastward dip of approximately 60°, and an azimuth of 340° (Figure 6.2c, 6.7a). This body is inferred to be the western limb of an anticlinal structure that has been identified at several places along the thrust. In the southern part of the Mooki Fault in the Manilla map sheet, the line LS_20 across the outcrop of the Tulcumba Ridge is modelled by two eastward dipping tabular or polygon bodies, suggesting the magnetic rocks are probably two east-dipping units within the anticline (Figure 6.6b). On the Tamworth map sheet, a ground magnetic profile (Breeza profile) was conducted at the northern edge of the Quirindi Dome and could be best matched by a single tabular body dipping to the east at 52° or by a structure with a western overturned limb and an eroded eastern limb of a westward overturned anticline. To the south of the line Breeza, the synthetic magnetic line LS_10 that crosses the southern part of the Quirindi Dome could be explained by a structure with an overturned western limb and a more shallowly dipping eastern limb of an overturned anticline. The anomaly could also be explained by a westward overturned anticline.

The magnetic modelling of this study has produced different results to the work of Ramsay and Stanley (1976). To a significant degree, the difference in the results can be explained in terms of magnetic sources, which produced the Mooki anomalies. Ramsay and Stanley (1976), on the basis of the modelling of the ground magnetic data collected north of the Tulcumba Ridge, suggest that the Mooki anomalies were produced by plug-like correlatives of the Warrigundi Igneous Complex in the south and a long dyke of hawaiite genetically related to the Nandewar alkaline volcanic complex in the north, and modelled the observed anomalies as a single tabular body. This interpretation of the new high resolution aeromagnetic data, incorporated with the recent work by Scheibner and Webster (1982), Schmidt (1994) and Greentree and Flood (1999), indicated that the anomalies are produced by the contrast between higher magnetic susceptibilities of the Currabubula Formation to those lower values of the Late Permian and Triassic sediments (Sydney-Gunnedah basin) to the west. Modelling of the magnetic profiles across the Mooki Fault indicates that the geometry of the Mooki Fault could not be simply modelled by a single tabular body parallel to the fault in all cases, and relatively complex geological structures need to be modelled to match the observed anomalies at Quirindi Dome. Lines extracted from high resolution aeromagnetic dataset across the Tulcumba and Quirindi Dome provide a chance to model the anomalies as a dome structure and confirmed that the magnetic anomalies are indeed consistent with that produced by an overturned dome structure as defined in the surface geology (Carey, 1934a, b; Liang, 1991).

Models developed in this study explained successfully the magnetic anomalies immediately east of the Mooki Fault. It needs to be stressed that the developed magnetic models represent the western edge of the Tamworth Belt, and do not image directly the Mooki Fault as is observed in the seismic survey (Korsch et al., 1993a, 1997), by which the Mooki Fault was imaged as a shallowly eastward dipping fault. The developed models are also

different from the model produced by Ramsay and Stanley (1976), who modelled the Mooki Fault with an eastward dip of 25° assuming that the modelled dyke was emplaced along the Mooki Fault. The modelling results in this study are consistent with a fault-propagation fold adjacent to the Mooki Fault at the west edge of the Tamworth Belt, which has a thrust step-up angle of ~30° from the décollement (Liang, 1991).